

A Multi-wavelength Study of the X-ray Sources in NGC 5018

Kajal K. Ghosh¹, Douglas A. Swartz¹, Allyn F. Tennant², Kinwah Wu³, and
Lakshmi Saripalli⁴

ABSTRACT

The E3 giant elliptical galaxy NGC 5018 was observed with the *Chandra* X-ray Observatory's Advanced CCD Imaging Spectrometer for 30 ks on 14 April 2001. Results of analysis of these X-ray data as well as of complementary optical, infrared, and radio data are reported. Seven X-ray point sources, including the nucleus, were detected. If they are intrinsic to NGC 5018, then all six non-nuclear sources have luminosities exceeding 10^{39} ergs s⁻¹ in the 0.5–8.0 keV energy band; placing them in the class of Ultra-luminous X-ray sources. Comparison of X-ray source positions to archival Hubble Space Telescope/Wide Field Planetary Camera 2 (*Hubble*/WFPC2) images reveal four of the six non-nuclear sources are spatially-coincident with bright, $M_V \lesssim -8.6$ mag, objects. These four objects have optical magnitudes and (V-I) colors consistent with globular clusters in NGC 5018 but they also have X-ray-to-optical flux ratios consistent with background active galactic nuclei. Strong, unpolarized, radio emission has been detected from one of the optically-bright counterparts. Another optically-bright counterpart was observed to vary by ~ 1 mag in optical observations taken 28 July 1997 and 04 Feb 1999. Extended X-ray emission is detected within a $\sim 15''$ radius of the galaxy center at a luminosity of $\sim 10^{40}$ ergs s⁻¹ in the X-ray band. Its thermal X-ray spectrum ($kT \sim 0.4$ keV) and its spatial coincidence with strong H α emission are consistent with a hot gas origin. The nucleus itself may be a weak X-ray source, $L_X \lesssim 3.5 \times 10^{39}$ ergs s⁻¹, that displays a radio spectrum typical of AGN.

¹Universities Space Research Association, NASA Marshall Space Flight Center, SD50, Huntsville, AL, USA

²Space Science Department, NASA Marshall Space Flight Center, SD50, Huntsville, AL, USA

³MSSL, University College London, Holmbury St. Mary, Surrey, RH5 6NT, UK

⁴Australia Telescope National Facility, CSIRO, Locked Bag 194, Narrabri, NSW 2390, Australia

1. Introduction

Chandra images of nearby galaxies routinely reveal dozens of discrete X-ray sources per galaxy above a detection threshold of $\sim 10^{37}$ ergs s $^{-1}$ (Fabbiano & White 2003). For many of these images, the population of Ultra-Luminous X-ray sources is a major focus of study (e.g., Roberts, & Warwick 2000; Kilgard et al. 2002; Humphrey et al. 2003; Irwin, Athey, & Bregman 2003; Irwin, Bregman, & Athey 2004; Colbert et al. 2004; Swartz et al. 2004).

Ultra-Luminous X-ray sources (ULXs) in nearby galaxies are non-nuclear point-like objects with X-ray luminosities $> 10^{39}$ ergs s $^{-1}$, above the Eddington limit for spherical accretion of hydrogen onto a $\lesssim 8 M_{\odot}$ object. ULXs must either accrete mass at a high rate or result from supernovae in very favorable circumstances in order to emit so copiously in the X-ray band. If ULXs are accretion-powered, then they are either massive – the elusive intermediate-mass black holes (IMBHs) (Colbert, & Mushotzky 1999; Makishima et al. 2000; Colbert & Ptak 2002; van der Marel 2003), or they emit anisotropically (with a true luminosity less than the isotropic equivalent) (King et al. 2001; Georganopoulos, Aharonian, & Kirk 2002) or they are truly super-Eddington (Abramowicz et al. 1988; Begelman 2002; Grimm, Gilfanov, & Sunyaev 2003). Alternatively, some ULXs, at least, may not be accreting objects but are associated with supernovae and hypernovae (Franco et al. 1993; Plewa 1995).

There is a growing consensus (Grimm, Gilfanov, & Sunyaev 2003; Colbert et al. 2004; Fabbiano 2004; Gilfanov 2004; Irwin, Bregman, & Athey 2004; Swartz et al. 2004), based on global properties of ULX host galaxies, that there are (at least) two populations of ULX: (1) A bright population associated with recent star formation with the number of ULXs and their X-ray luminosities scaling with their host galaxy’s far-infrared luminosity and other tracers of star-formation rate; and (2) A population of weaker ULXs (perhaps not exceeding $\sim 2 \times 10^{39}$ ergs s $^{-1}$, Irwin, Bregman, & Athey 2004) found in early-type galaxies with a population proportional to blue luminosity and other galaxy mass indicators. Thus, ULXs are likely to be a heterogeneous group of high-mass X-ray binaries (XRBs) and supernovae, products of recent star formation and found primarily in late-type galaxies, and low-mass XRBs (LMXBs) in the late evolutionary stages of the mass donor star, accounting for ULXs in ellipticals (see also King 2002).

This dichotomy implies the ULX population in the E3 galaxy NGC 5018 should be composed of LMXBs of luminosity $\lesssim 2 \times 10^{39}$ ergs s $^{-1}$ with the number of ULXs scaling with blue luminosity, L_B . We find twice as many ULX candidates as expected and 3 of the 6 candidates have observed luminosities $> 2 \times 10^{39}$ ergs s $^{-1}$ in the 0.5-8.0 keV band. While not beyond statistical chance, this result was remarkable enough that closer inspection of the ULX population of NGC 5018 was undertaken and is reported here. Archival *Chandra*, *Hubble*, 2MASS, newly acquired radio observations and data reduction techniques are pre-

sented in § 2. Individual ULX candidates are described in § 3 and the nature of the nucleus and diffuse emission is considered in § 4. The possible origin of the X-ray emission and its implication for the recent evolution of NGC 5018 is discussed in § 5.

2. NGC 5018 Observations and Data Reduction

The type E3 giant elliptical galaxy NGC 5018 is the brightest member ($M_B = -21.45$ mag) of a group of 5 galaxies located at a distance of 40.8 Mpc ($1'' = 198$ pc). NGC 5018 is connected to its two nearest neighbors, NGC 5022 and MCG 03-34-013 (see Figure 1), by a large H I bridge that supplies gas to NGC 5018 (Kim et al. 1988; Guhathakurta et al. 1989). There is also a distinct stellar bridge between NGC 5018 and NGC 5022 and an embedded dust lane in NGC 5018; both relics of a past interaction (Malin & Hadley 1997). Further evidence of its dynamic history are shells around the galaxy, a tidal tail (Malin & Carter 1983), and a compact radio core (Mollenhoff et al. 1992). The interaction is estimated to have occurred 300 to 600 Myr ago (Guhathakurta et al. 1989).

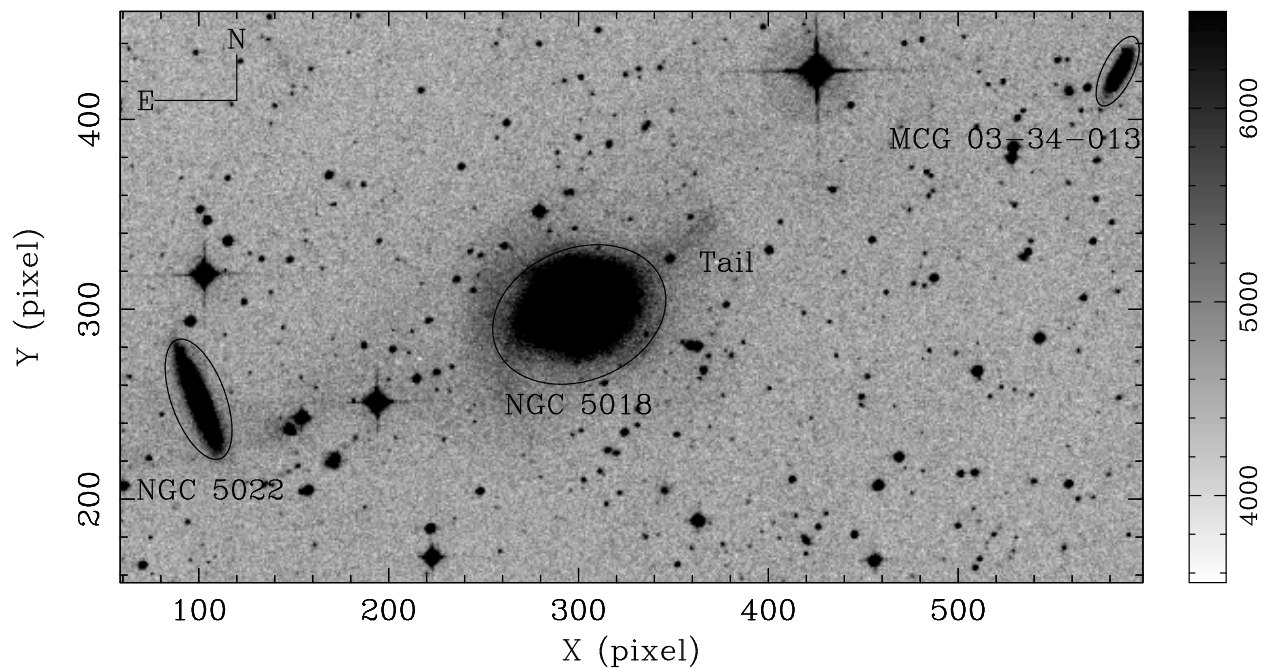


Fig. 1.— Optical Digitized Sky Survey (red) image of NGC 5018. A stellar bridge lies between NGC 5018 and NGC 5022 and a tidal tail is present on the opposite side of this bridge. D_{25} isophotes (defined as the major isophotal angular diameter measured at a blue light surface brightness level of $25.0 \text{ mag sec}^{-2}$) are shown around NGC 5022, NGC 5018 and MCG 03-34-013. The image is approximately 16.4×10.5 arcmin

2.1. X-ray Observations

A 30 kilosecond observation of NGC 5018 was carried out with the *Chandra* Advanced CCD Imaging Spectrometer (ACIS) operating in imaging mode on 2001 April 14 (ObsID 2070). This dataset was retrieved from the *Chandra* archive and the Level 2 event list was used to extract the events within the $3.3 D_{25}$ isophote of NGC 5018 (fully within the back-illuminated CCD S3). Source detections and source and background light curves and spectra were extracted using the locally-developed software package `lextrct` (Tennant et al. 2005). Some details of data reduction methods are given in Swartz et al. (2003).

The detection limit for point sources in this observation is $\sim 6 \times 10^{38}$ ergs s^{-1} , assuming an absorbed power-law of photon index $\Gamma = 1.8$ (the average for ULXs in the sample considered by Swartz et al. 2004), the Galactic absorption column along the line of sight ($N_H = 6.98 \times 10^{20}$ cm^{-2}), and a 10 c detection limit. Figure 2 shows the *Chandra* image of NGC 5018 in the 0.5 to 8.0 keV band with $2''$ radius circles about the detected source locations. Seven sources (including the nucleus) were detected within the D_{25} region above a signal-to-noise ratio of 2.8. Table 1 lists the *Chandra* positions, X-ray spectral fit parameters, 0.5–8.0 keV absorption-corrected luminosities, X-ray colors, and total detected counts for each source.

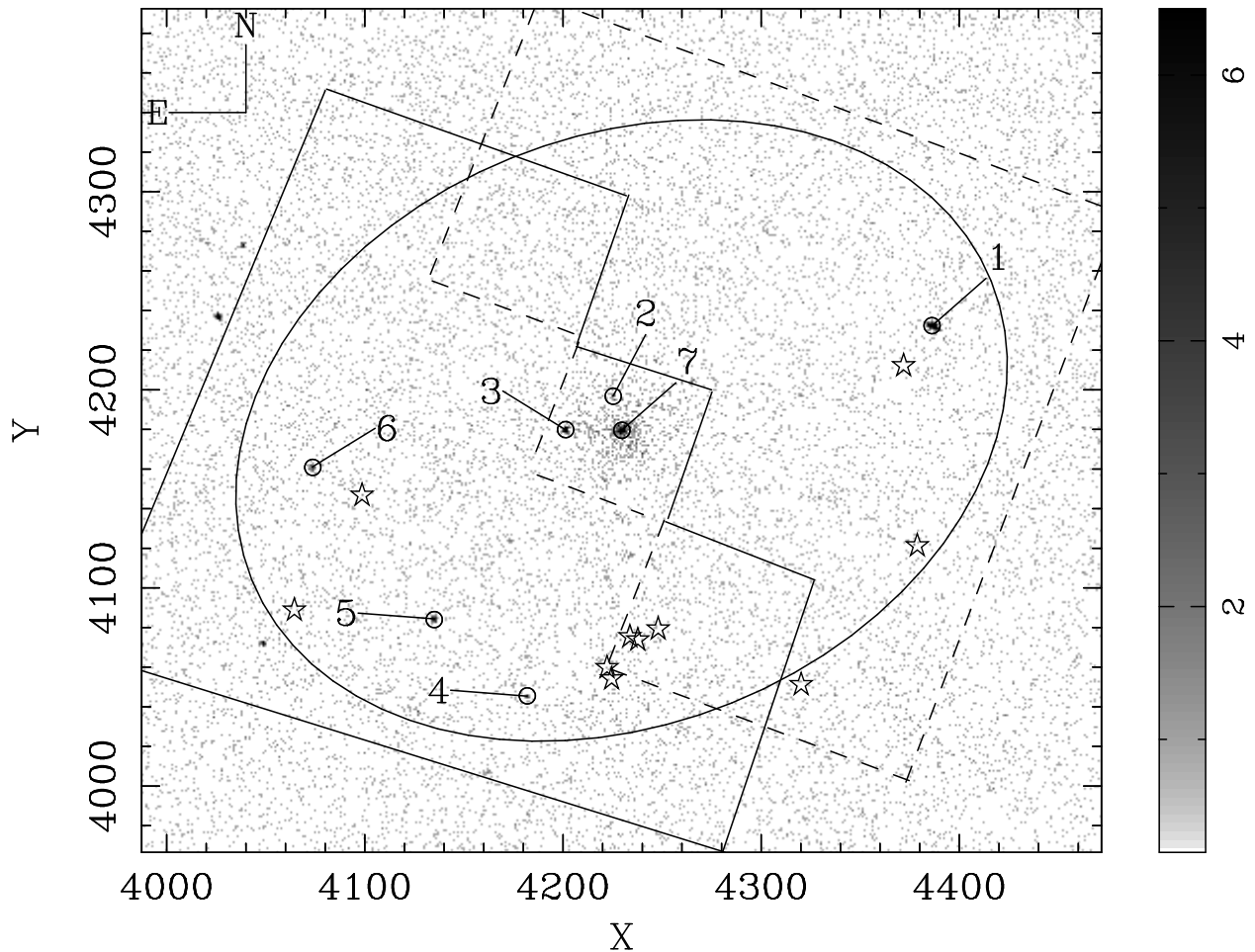


Fig. 2.— *Chandra* image of NGC 5018 in the 0.5 to 8.0 keV band. The ellipse denotes the $D_{25}=3.3'$ isophote. The bright nucleus is surrounded by diffuse emission extending to $\sim 10''$. The seven detected point sources are indicated with $2''$ radius circles. Solid lines depict the boundaries of available *Hubble*/WFPC2 images observed with F555W (4400 s) and F814W (5240 s) filters and dashed lines depict the orientation used for F336W (1800 s), F555W (1200 s), and F814W (1900 s) images, see Table 2. Ten USNO astrometric stars are shown with star symbols. (Two other USNO stars lying very close to the nucleus are not shown) The image is approximately 4.1×3.5 arcmin.

The centroids of the source positions were determined by fitting an elliptical Gaussian to the spatial distribution of X-ray events. The estimated statistical uncertainty in the source positions was computed from the ratio of the size of the point spread function and the square root of the source counts. These values are between 0."05 and 0."13.

The 3 brightest sources, including the nucleus, produced enough X-ray counts for spectral analysis. For these sources, spectral redistribution matrices and ancillary response files were generated using CIAO, v2.3, and models were fitted to their 0.5 to 8.0 keV energy spectra, binned to obtain at least 10 c per fitting bin, using XSPEC v11.3. Parameters for the best-fitting models are listed in Table 1 and discussed more fully in § 3 and 4. The X-ray light curves for these three sources were also extracted, using 500 s binning, and tested against the constant countrate hypothesis.

The 0.5-8.0 keV X-ray luminosities are estimated from model fits to the brightest sources or by assuming a $\Gamma = 1.8$ absorbed power law and the Galactic N_H value of $7 \times 10^{20} \text{ cm}^{-2}$ in the direction of NGC 5018, for the weaker sources using PIMMS (Mukai 1993).

2.2. Optical Observations

A log of archival *Hubble*/WFPC2 observations of NGC 5018 is given in Table 2. Exposure calibrated and co-added cosmic ray free WFPC2 images were retrieved from the WFPC2-Associations¹ database for analysis. Positions of the *Hubble* images of NGC 5018 relative to the *Chandra* image are outlined in Figure 2.

The nucleus is the only catalogued object common between the *Hubble* and *Chandra* images and it was used to register the two images assuming the centroids of the optical and X-ray emission coincide. The uncertainties of the best-fit elliptical Gaussian to the X-ray nucleus is $\sim 0."05$ and we take this to be the registration uncertainty for the two ULX candidates lying on the *Hubble*/PC1 image. This uncertainty is combined in quadrature with the (statistical) uncertainties in the X-ray positions of these two sources to give their final positional uncertainties as listed in Table 3.

For the remaining ULX candidates there is an additional uncertainty in the registration because these sources lie on the outer *Hubble*/WF (WF2, WF3, and WF4) CCDs. This additional uncertainty was estimated using the METRIC program². The images of the ten

¹<http://archive.stsci.edu/hst/wfpc2/>

²<http://stdas.stsci.edu/cgi-bin/gethelp.cgi?metric.hlp>

USNO stars on these CCDs along with two USNO stars on PC1 were used to determine this uncertainty. First we noted the differences between the USNO catalog and the *Hubble* values of the positions of the two USNO stars on the PC1 image and computed the average offset. We then applied this average value as the offset to the WF images and determined the differences between the catalog and the *Hubble* values of the USNO stars located on the WF images. These values are then considered as the relative positional errors between the PC and WF images, which range between 0."17 and 0."33 for the three CCDs. This results in slightly larger uncertainties for the ULX candidates lying on these CCDs as can be seen from Table 3.

A potential optical counterpart was discovered within the resulting error circles for four of the candidate ULXs in at least two *Hubble* image bands. The other two ULX candidates have only upper limits in V and I. The upper limit values were determined by centering on the brightest pixel within or nearest to the error-circle. The difference in counts obtained from a circle of 3-pixel radius and that obtained from an annulus of 3 and 5 pixel radii, were used as the upper limit count of the optical counterpart of the ULX candidate. The resulting observed magnitudes, aperture-corrected using the curve of growth method, are listed in Table 3. Also listed are the absolute V-band magnitudes assuming distance modulus = 33.1 mag and corrected for Galactic extinction, optical colors, and the X-ray-to-optical flux ratios (F_X/F_O). F555W-band magnitudes of the ULX candidates were used to compute the values of F_O using the current values of PHOTFLAM and Zeropoint in the VEGAMAG system given in the *Hubble* data handbook for WFPC2³. For brevity, we will refer to F336W, F555W, and F814W as U, V and I, respectively.

Measured fluxes were consistently lower in the association dataset U3M72505B when compared to the U3M72508B data. We downloaded the component datasets that went into both associations and found consistency at that level. Thus it appears that the U3M72505B association dataset has been incorrectly processed and we have ignored this dataset and used our own processing of its component files. We also found that the F336W band association data (U2ST0201B) still showed obvious cosmic ray tracks. Again we downloaded the component files and reprocessed the data which effectively removed the cosmic rays. This did not change the measured flux for ULX 3, but it did produce a better looking figure.

³http://www.stsci.edu/instruments/wfpc2/Wfpc2_dhb/wfpc2_ch52.html # 1902177

2.3. Radio observations

We have carried out radio observations of NGC 5018 using the Australia Telescope Compact Array (ATCA). We measured radio continuum flux data in total and polarized intensity on June 30, 2004, simultaneously observing at four frequencies, 1.4, 2.3, 4.8 and 8.6 GHz. The nucleus and the ULX candidate # 6 were both detected at high significance.

In addition, low resolution 20 cm continuum and H I λ -21 cm (Kim et al. 1988) and high resolution 20 cm continuum observations (Mollenhoff et al. 1992) of NGC 5018 were carried out with the Very Large Array of the National Radio Astronomy Observatory. These observations also detected radio emission from the nucleus and at the location of source # 6. Results of these measurements are given in Table 5. There are no radio sources in the NRAO/VLA Sky Survey catalog near the locations of the other ULX candidates. These regions have not been covered by the FIRST survey.

2.4. Infrared observations

J, H and K_s band images of NGC 5018 were retrieved from the 2MASS archive. After inspecting these images around the positions of the ULX candidates, we decided to analyze only the K_s band image as it is of the highest quality. The astrometry between the 2MASS and *Chandra* images was done using the nucleus as a registration object. No prominent sources were detected at the positions of the ULX candidates.

3. Non-nuclear X-ray sources

All six non-nuclear X-ray sources are potential ULXs assuming they are within the host galaxy. Four sources are spatially-coincident with potential optical counterparts and upper limits to the optical brightness are made for the remaining two sources as described in the following subsections. The high measured values of F_X/F_O suggests neither of these two optically-weak sources are foreground stars nor background AGNs (Maccacaro et al. 1988). For the four sources with well-defined optical counterparts, $F_X/F_O \sim 1$ which is typical of AGNs (Green et al. 2004; Veron-Cetty & Veron 2003). Statistically, we expect about 1.4 background AGNs among our detected sources based on the *Chandra* deep field studies (Brandt et al. 2001). However, as discussed below, the counterpart optical colors and brightnesses are also consistent with globular clusters within NGC 5018. Before discussing the individual sources in detail, we present X-ray color-color (§ 3.1) and optical color-magnitude (§3.2) diagrams for the entire population of detected X-ray sources.

3.1. X-ray color-color diagram

The background-subtracted X-ray colors are defined as $(M - S)/T$ and $(H - M)/T$, where $T = S + M + H$ and S , M , and H denote counts in the 0.5-1.0 keV, 1.0-2.0 keV, and 2.0-8.0 keV bands, respectively, extracted from $\sim 90\%$ encircled energy radii. X-ray colors are listed in Table 1. Total detected counts, T , are given at the last column of Table 1. Figure 3 displays the X-ray color-color distribution of the seven sources. Five sources are located at the position of mildly absorbed X-ray binaries (Prestwich et al. 2003) and are otherwise non-descript. Source # 6 appears to be extremely hard and occupies a region in the color-color diagram where the spectrum is very flat (compare Figure 4 of Prestwich et al. 2003). This source is also a strong radio source. The nucleus of NGC 5018, in contrast, is very soft. This is mainly due to the presence of a strong thermal component, as discussed in § 4.

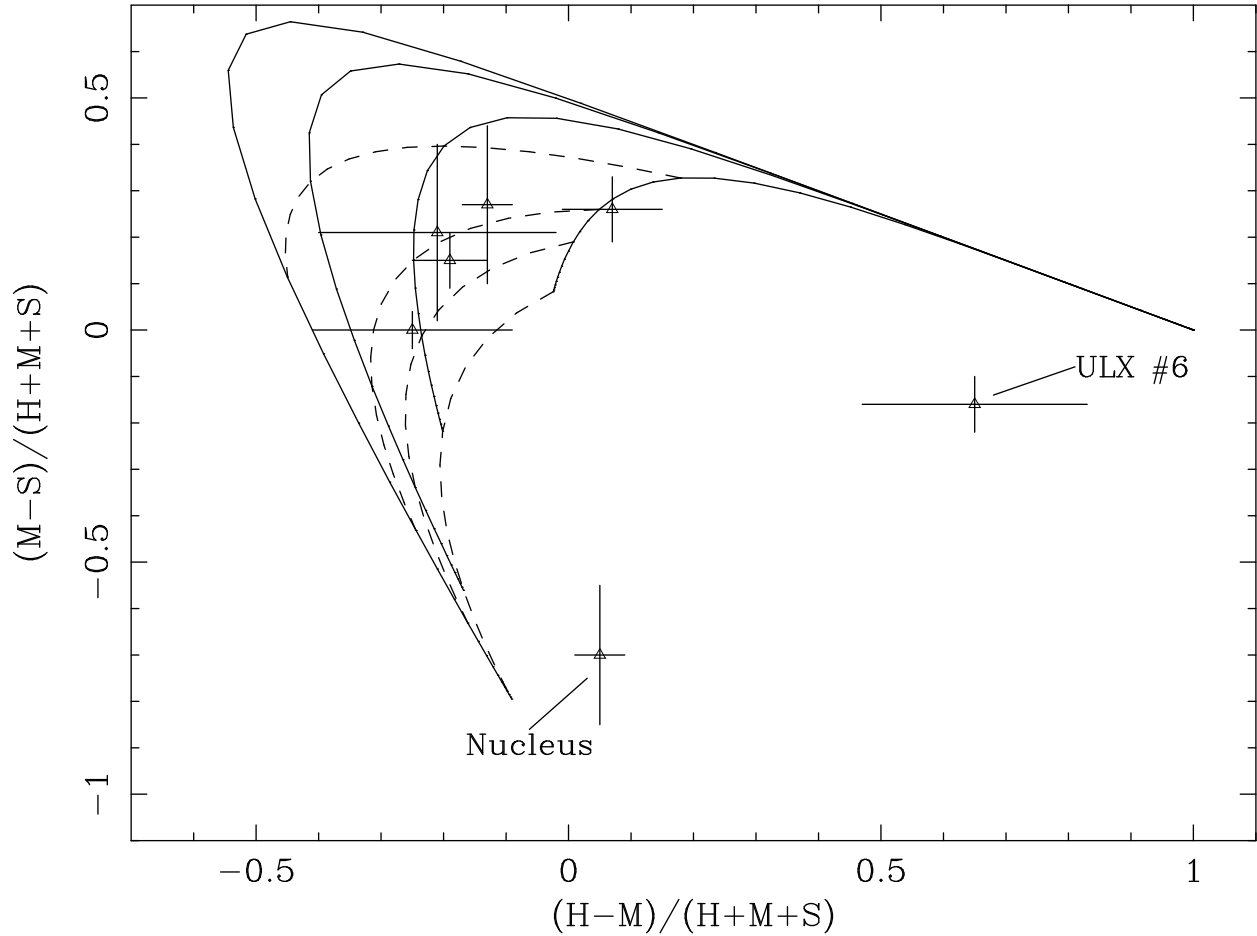


Fig. 3.— X-ray color-color diagram of point sources in NGC 5018. Solid curves denote colors of absorbed power law models of spectral indices $\Gamma=1,2,3$, and 4 (from right to left) and for the range of absorbing columns $n_H=10^{20}$ to 10^{24} cm^{-2} . Dashed curves denote constant absorption columns of $n_H=10^{20}$, 10^{21} , 2×10^{21} , and 5×10^{21} cm^{-2} (from bottom to top). Errors shown were propagated from the statistical uncertainties in the three X-ray bands.

3.2. Optical color-magnitude diagram

The absolute V band magnitude (M_V) is shown against the (V–I) color for the six possible optical counterparts to the non-nuclear sources in Figure 4. Four of the counterparts are much brighter than individual stars. All four of these counterparts are as bright or brighter than globular clusters (GCs) in the Milky Way (Harris 1996) indicating they are massive compact GCs analogous to some of those found in other nearby galaxies. In contrast, only upper limits were obtained for any counterparts to sources # 1 and # 4.

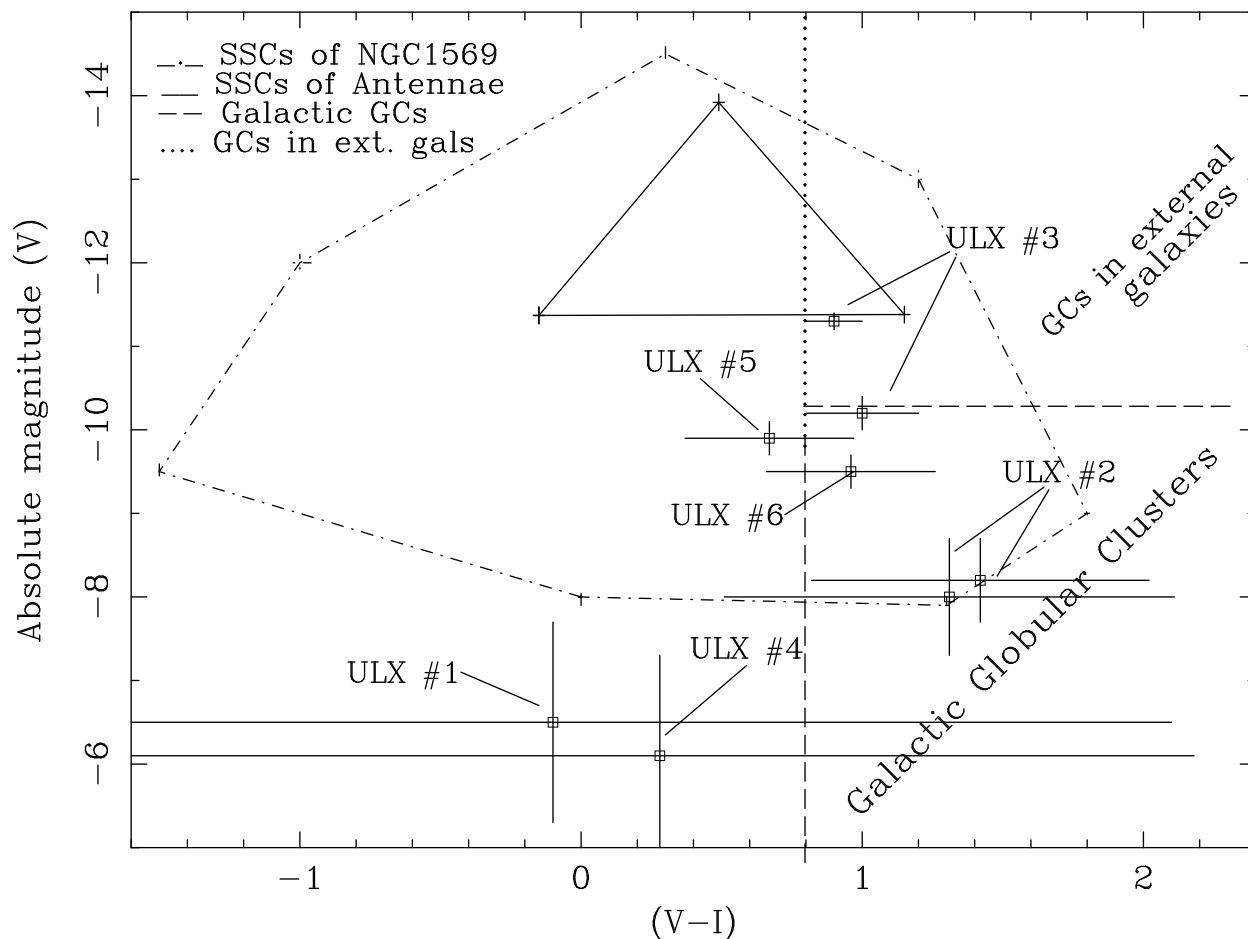


Fig. 4.— Absolute magnitude in V-band versus (V-I) color for the counterparts of the six non-nuclear X-ray sources detected in NGC 5018. Known globular clusters lie to the right and super star clusters to the left, respectively, of a line roughly at (V-I)=0.8. The dashed lines denote the region occupied by Galactic globular clusters on the lower right (Harris 1996). Globular clusters in other galaxies can be much brighter (e.g., Miller et al. 1997; Lotz et al. 2004) and extend the globular cluster region to the upper right. Domains of super star clusters detected in the Antennae (Whitmore et al. 1999), and in NGC 1569 (Hunter et al. 2000) are also shown. Note the overlap into the red color space occupied by globular clusters. Two points are plotted for the counterparts to source # 2 and # 3 corresponding to the two separate HST observations.

Also shown in Figure 4 are the regions of color-magnitude space occupied by super star clusters (SSCs) in some well-studied star-forming galaxies. SSCs are compact, luminous star clusters that have sizes and luminosities comparable to GCs but are relatively much younger ($\lesssim 1$ Gyr) and bluer than GCs. They tend to lie blueward of $(V-I) \sim 0.8$, as indicated in Figure 4, though there is substantial overlap among the two classes. The NGC 5018 GC survey undertaken by Hilker & Kissler-Patig (1996) discovered at least two populations of GC: a blue population with $\langle V-I \rangle \sim 0.7$ (about 10% of all GCs) and a broader red population with $(V-I) \gtrsim 1.0$. Hilker & Kissler-Patig (1996) attribute the blue population to those GCs formed within the last few 100 Myr to 6 Gyr while the red population is an older primordial population. It should be noted that the $(V-I)$ colors alone cannot discriminate between age and metallicity effects. The blue clusters may simply be old metal-poor clusters (perhaps captured from another galaxy in a merger or interaction).

Four bright optical counterparts to X-ray sources have $(V-I)$ colors overlapping with this population of blue GCs in NGC 5018. They are also within the $(V-I)$ color range of AGNs (~ 0 to ~ 2 ; e.g., Zaggia et al. 1998). In fact, the optical counterpart to source # 3 (§ 3.5) varied by ~ 1 mag at optical wavelengths suggesting it is a background source and not a GC.

3.3. ULX Candidate 1

Source # 1 is the brightest X-ray object among the six ULX candidates detected in NGC 5018. The X-ray spectrum of this source is best described as an absorbed power law. Its intrinsic (absorption-corrected) luminosity in the 0.5–8.0 keV band is $(1.29 \pm 0.17) \times 10^{40}$ erg s $^{-1}$. It is not a highly absorbed source, because the value of N_H is consistent with the Galactic N_H .

The X-ray lightcurve of source # 1 is shown in Figure 5. The source is variable at a 94% confidence level during the *Chandra* observation according to the χ^2 test against a constant flux hypothesis ($\chi_r^2 = 1.3$ for 62 degrees of freedom). However, the Kolomogorov-Smirnov test, which is sensitive to longer term variability, gave a probability 0.85 indicating the source was almost constant. Thus, any short term variability was averaged out over the duration of the observation.

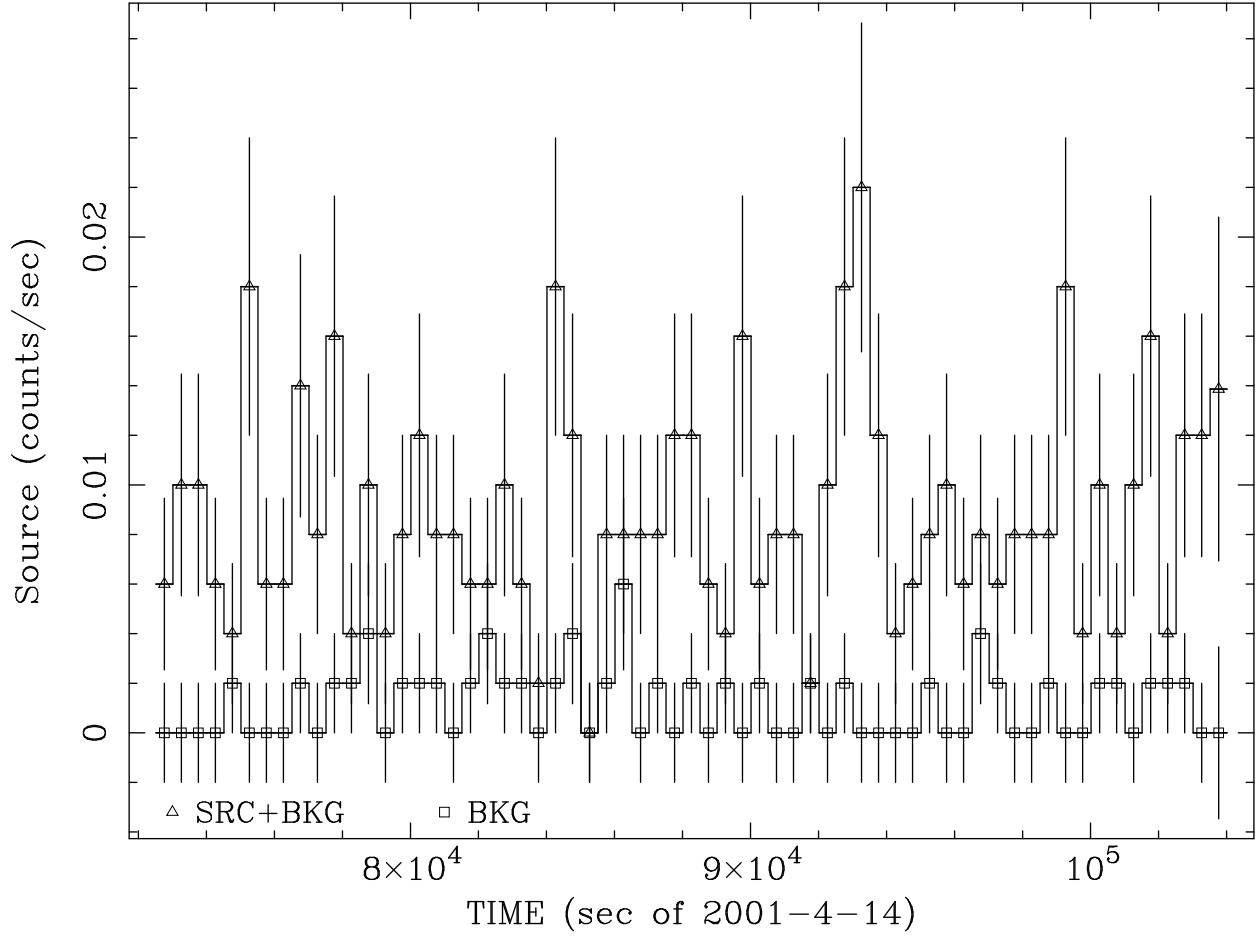


Fig. 5.— X-ray lightcurve of source # 1 with 500 s binning. The upper curve shows the combined source and background count rate (triangles) and the lower curve displays the local background count rate.

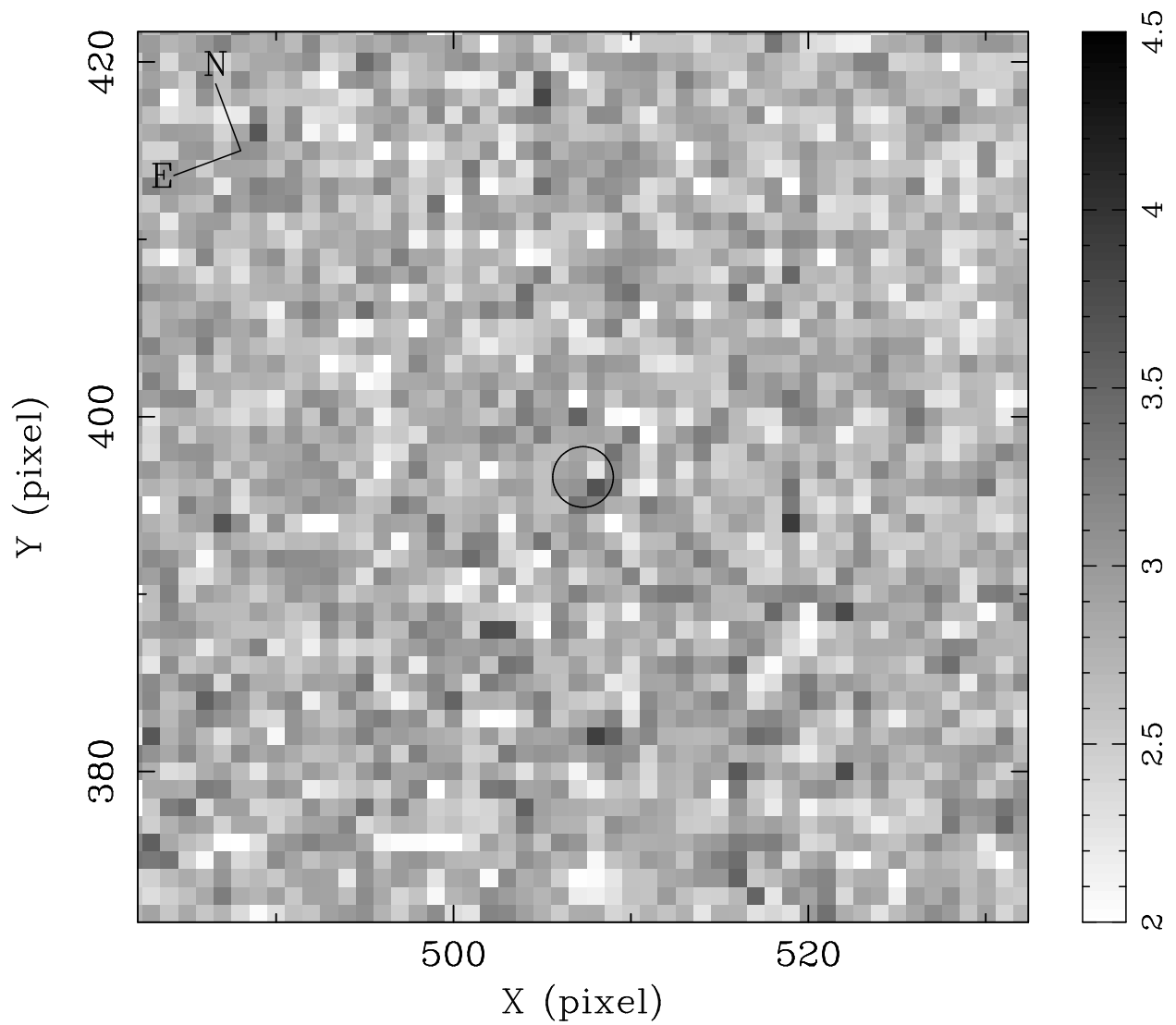


Fig. 6.— *Hubble* $5'' \times 5''$, 1200 s exposure, F555W band image centered on the ULX candidate # 1. The $0.17''$ *Chandra* error circle is also shown. There is about a 5 percent chance of finding a source as bright as the one in the error circle.

There is a weak source within the X-ray error circle of source # 1 in both the V and I *Hubble* images (Figure 6). However, several other nearby pixels show similar brightness levels and the object within the error circle may simply be caused by statistical fluctuations in the NGC 5018 field. It should therefore be considered as an upper limit to any optical counterpart to source # 1. Note that the measured absolute magnitude, $M_V = -6.5 \pm 1.2$, still exceeds that for all individual stars except for the brightest early-type supergiants. We note that the faintest globular clusters seen in our Galaxy have a similar brightness (Harris 1996).

3.4. ULX Candidate 2

Only 18 photons were detected from the *Chandra* image of source # 2 corresponding to an intrinsic luminosity of $(1.0 \pm 0.4) \times 10^{39}$ erg s⁻¹. Its X-ray colors are unremarkable (see Figure 3). A potential optical counterpart is present in the *Hubble* V and I images within 0."10 of the *Chandra* position.

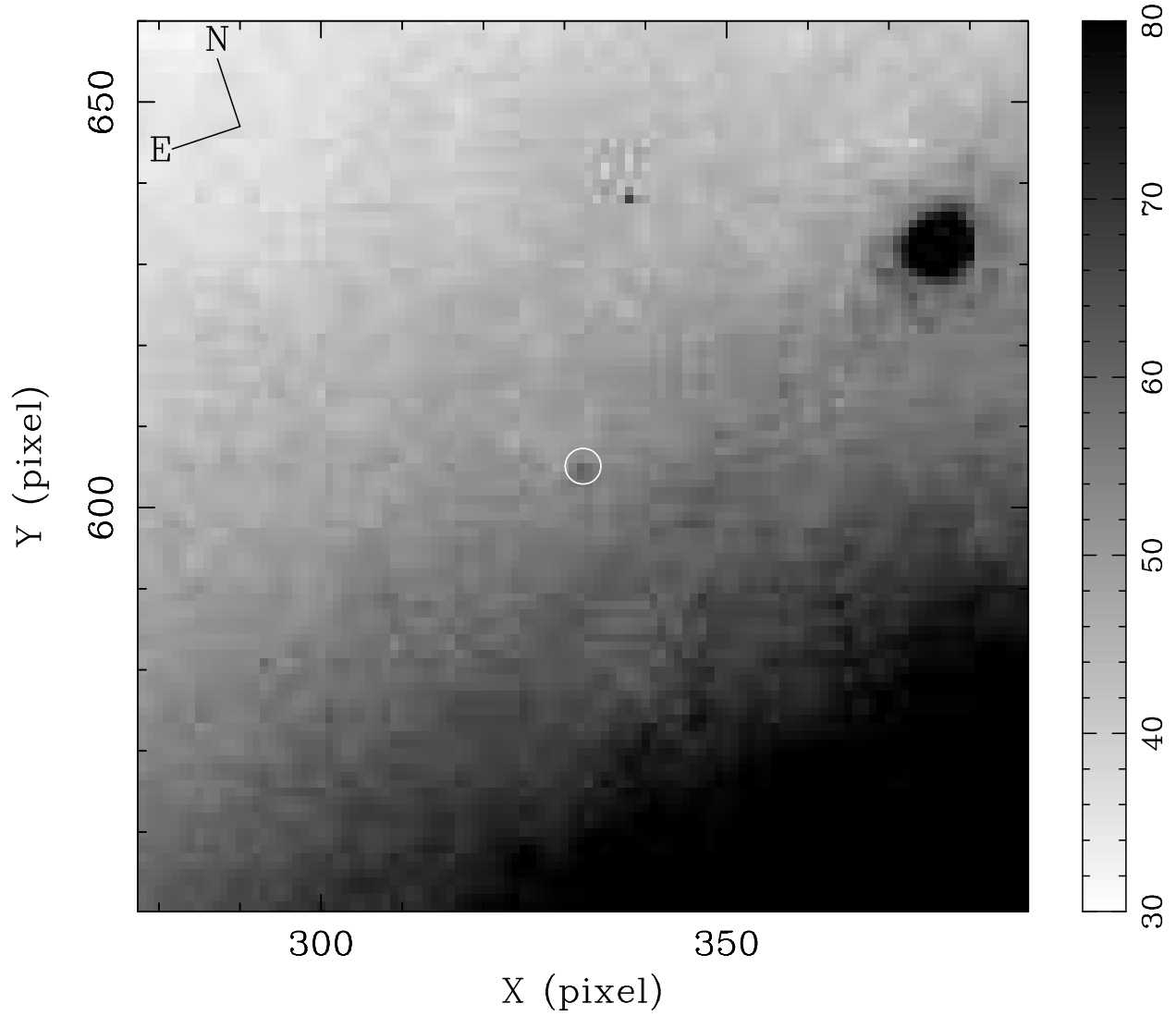


Fig. 7.— *Hubble* $5'' \times 5''$ F814W band PC1 camera image (5240 s integration) around ULX candidate # 2. After astrometric corrections, the positional offset between the *Hubble*-counterpart and the ULX candidate# 2 is $0.''10$. The circle depicts the $0.''1$ radius *Chandra* error circle.

Figure 7 shows a portion of the I band *Hubble* image with the 0."15 *Chandra* error circle superposed. The source is close to the bright nucleus and this accounts for the large gradient visible in the field surrounding the source. This source was observed on two occasions with the HST/PC1 camera and no variability was detected. The M_V and (V-I) values obtained for the counterpart (Figure 4 and Table 3) are consistent with those of Galactic globular clusters. Thus, source # 2 could be a ULX within a globular cluster in NGC 5018.

3.5. ULX Candidate 3

Source # 3 is bright enough in X-ray light to constrain its spectral shape. The X-ray spectrum is that of a modestly-absorbed power law (Table 1) with no other distinguishing spectral characteristics or unusual X-ray colors (Figure 3).

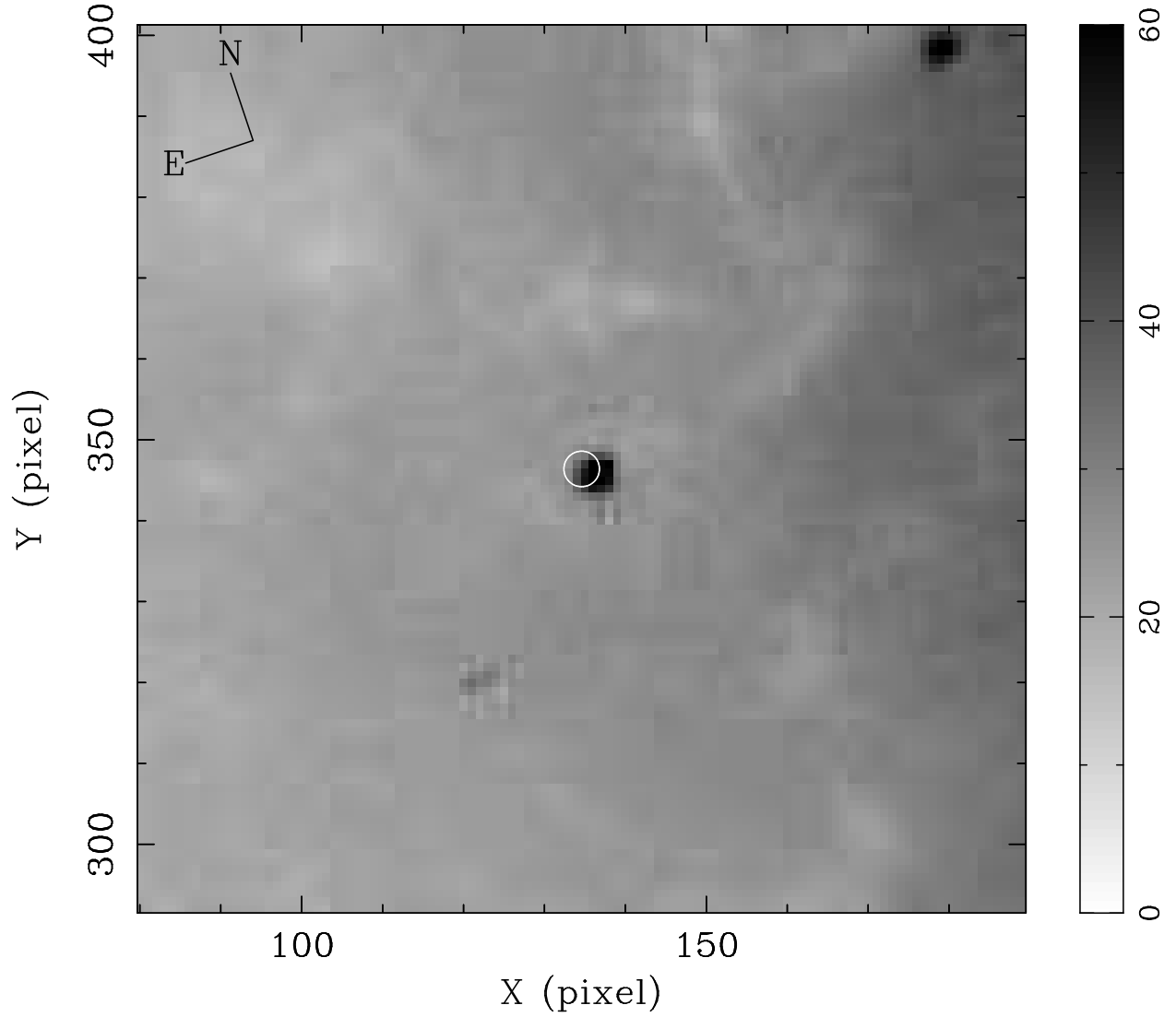


Fig. 8.— $5'' \times 5''$ region of the 4440 s *Hubble* F555W band PC1 image around the ULX candidate # 3. The *Hubble* object is $0.''1$ from center of the *Chandra* position at the edge of the *Chandra* error circle.

The optical object at the location of source # 3 is the only counterpart detected in all three *Hubble* filters. Figure 8 shows the V band *Hubble* image and Figure 9 the U band image. The region of NGC 5018 containing source # 3 was observed twice in V and I bands and once in U (Table 2). Table 3 shows that the counterpart to source # 3 varied in both V and I by about 1 mag between observations. Since the U band observations were not contemporaneous with either of the the V and I observations, we cannot make meaningful estimates of the (U–V) or (U–I) colors of the counterpart to source # 3.

The (V–I) color indicates the object is on the blue side of typical globular clusters and bordering on the SSC region (Figure 4). However, the variability is inconsistent with GC (or SSC) behavior. The F_X/F_O ratio is of order unity (Table 3) whereas foreground stars have lower values (Maccacaro et al. 1988). We conclude, therefore, that source # 3 is most likely a background AGN.

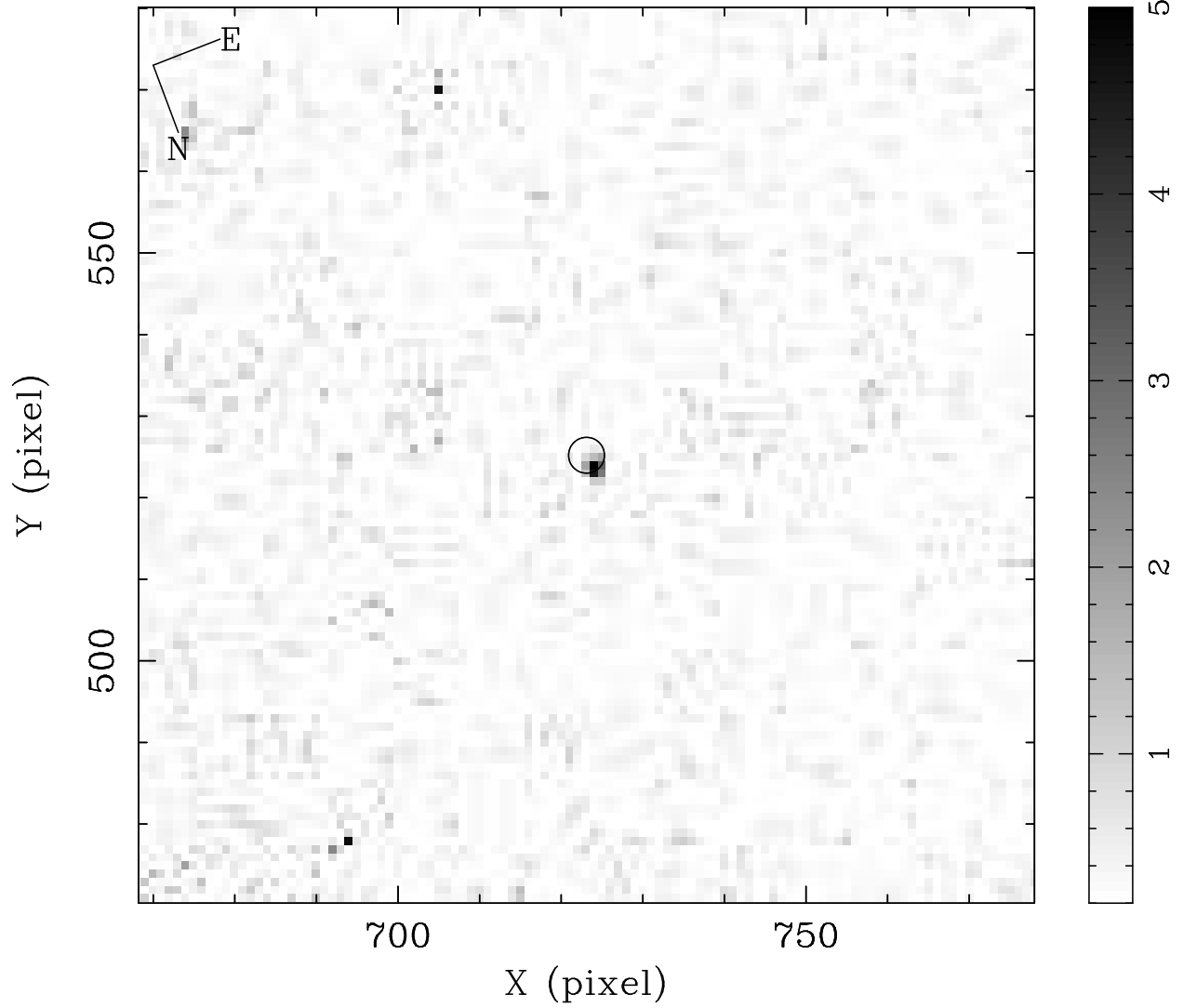


Fig. 9.— $5'' \times 5''$ region of the 1800 s *Hubble* F336W band PC1 image around the ULX candidate # 3. The *Hubble* object is $0.''1$ from center of the *Chandra* position at the edge of the *Chandra* error circle.

3.6. ULX Candidate 4

Source # 4 is another weak X-ray emitter with non-distinct X-ray colors. No obvious optical counterpart can be discerned from either the available *Hubble* V (Figure 10) or I band images of the field and only upper limits to a potential counterpart are listed in Table 3. In this regard, it is similar to source # 1 though source # 1 is much brighter in X-rays than source # 4.

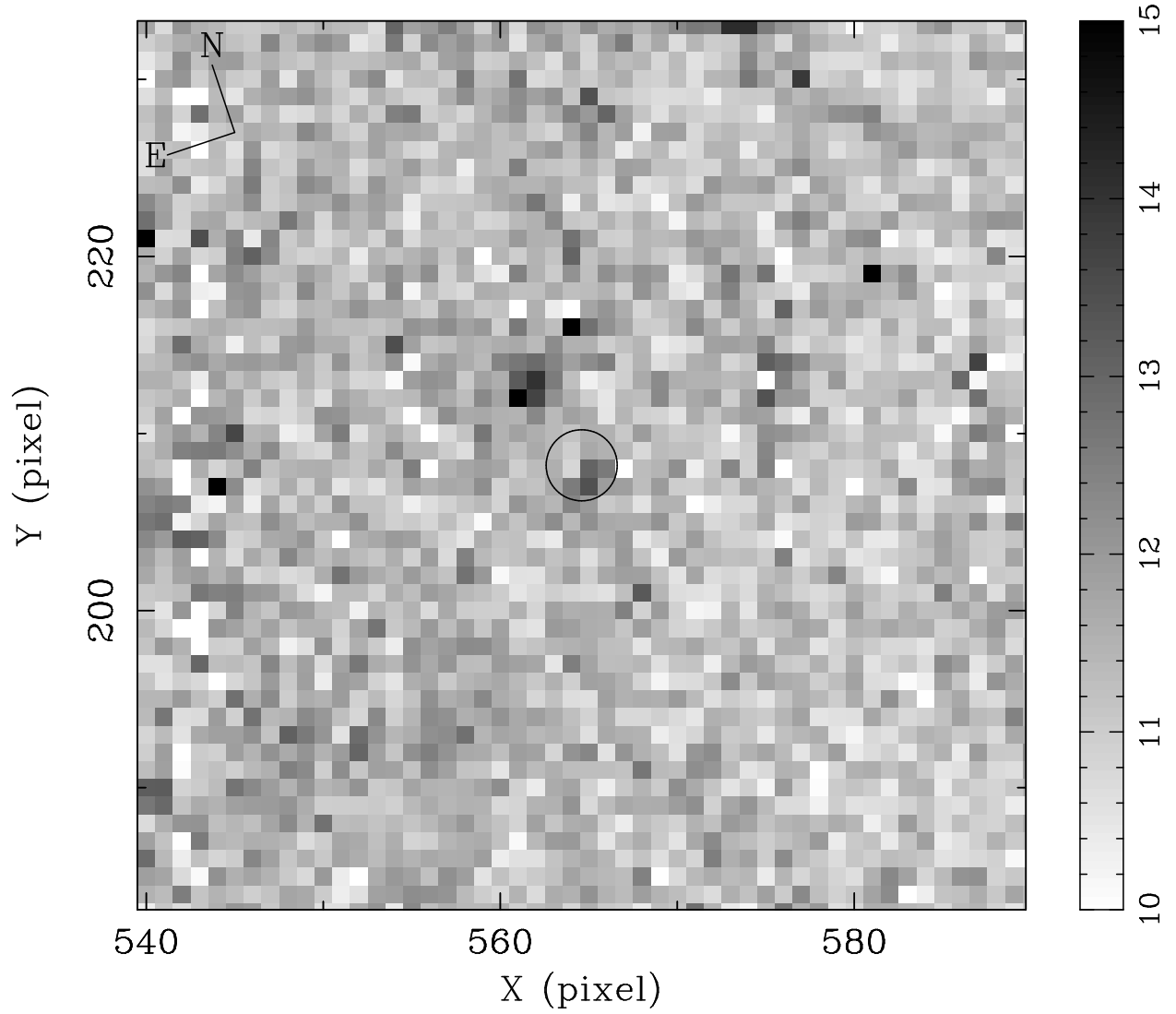


Fig. 10.— $5'' \times 5''$, 4440 s *Hubble* F555W image around ULX candidate # 4 with the $0.20''$ radius *Chandra* error circle added. There is about a 2.5 percent chance of finding a source as bright as the one in the error circle.

3.7. ULX Candidate 5

Source # 5 is moderately weak in X-rays with 42 counts detected. This corresponds to an intrinsic X-ray luminosity of $(2.4\pm 0.3)\times 10^{39}$ ergs s^{-1} . A potential counterpart was detected in both V and I images. After applying astrometric corrections, the positional difference between the counterpart and the ULX candidate is $0.''20$. Figure 11 shows the V band *Hubble* image in the vicinity of ULX candidate # 5. The location of the counterpart of ULX # 5 in Figure 4 suggests that it may be either a GC or a SSC in NGC 5018 or a background AGN.

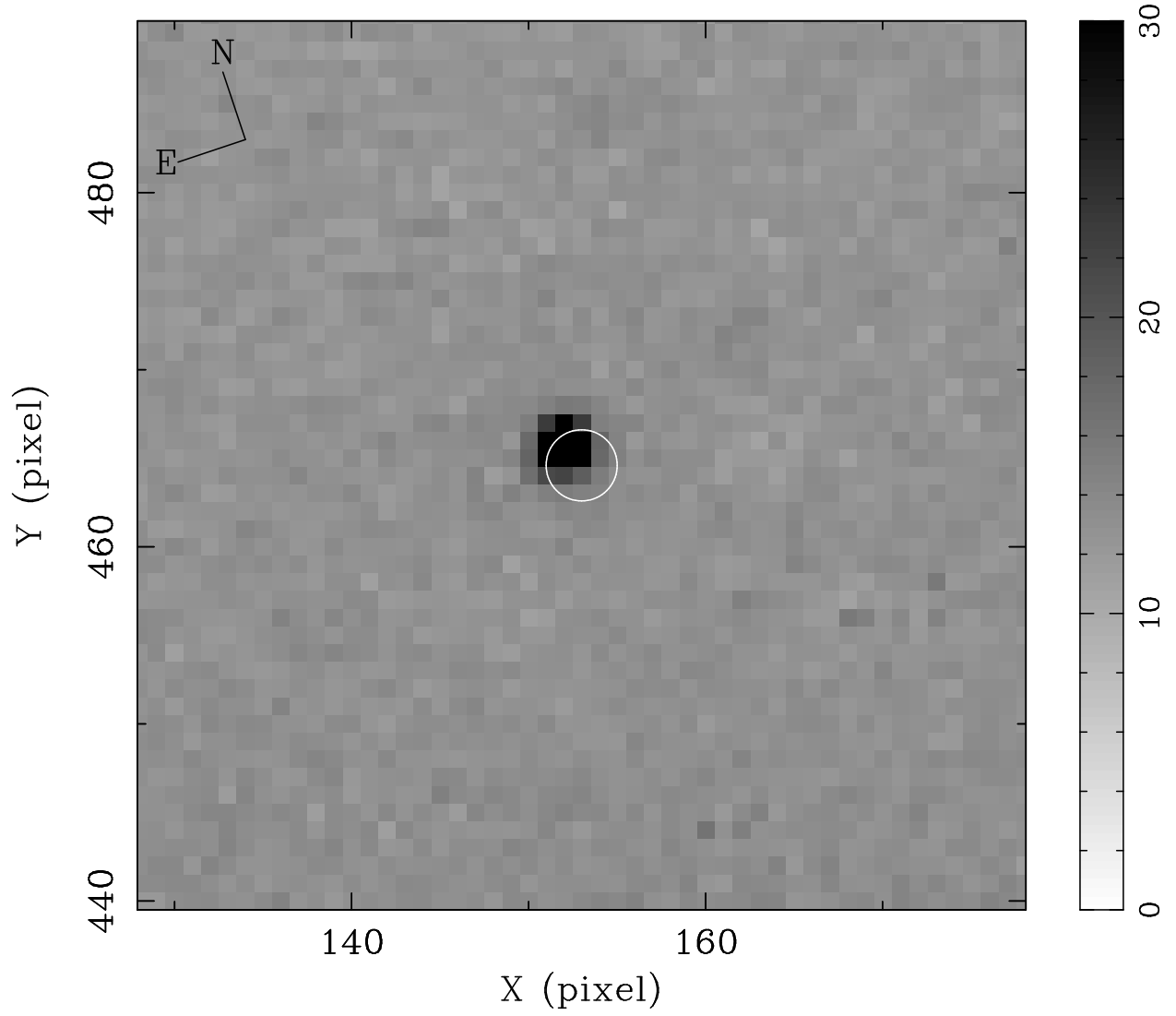


Fig. 11.— $5'' \times 5''$ F555W band image around the position of ULX candidate # 5. The $0.''2$ *Chandra* error circle encompasses a bright *Hubble* source.

3.8. ULX Candidate 6

Source # 6 is a weak X-ray source but is distinguished by an extremely hard X-ray spectrum as evidenced by its position in the X-ray color-color diagram (Figure 3). Although the X-ray colors suggest a very flat spectrum, the low S/N data does not allow us to rule out a more-typical power law index of $\Gamma \sim 1.8$. The region around this source was imaged only in the V and I filters. After astrometric corrections were applied to these images, a bright source was detected within $0.''2$ from the *Chandra* location (Figure 12). The optical source is similar to the other bright ULX counterparts in that it has a color and magnitude consistent with a globular cluster in NGC 5018.

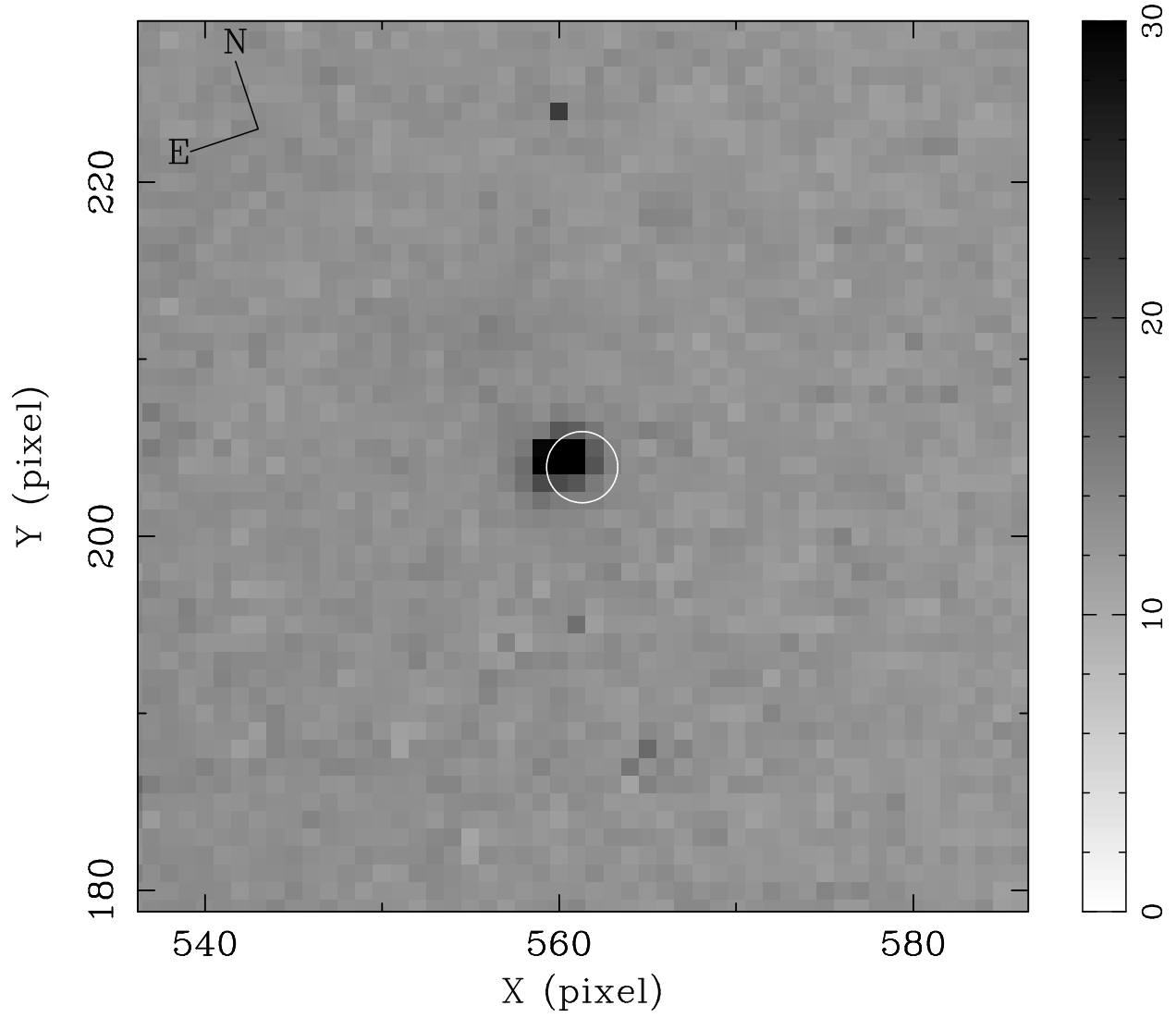


Fig. 12.— $5'' \times 5''$ F555W band image around the position of ULX candidate # 6. The $0.''2$ *Chandra* error circle encompasses a bright *Hubble* source.

Unlike all other ULX candidates in the NGC 5018 field, high-resolution radio data confirms (Mollenhoff et al. 1992) the detection of a radio source (Kim et al. 1988) at the position of source # 6 (see Table 5). After applying astrometric corrections based on the X-ray and radio positions of the nucleus, the position of the radio source is within $0.''15$ of the *Chandra* position of source # 6. This was confirmed through our multi-wavelength radio observations obtained with the Australia Telescope Compact Array (ATCA). We obtained radio continuum data in total and polarized intensity on June 30, 2004, simultaneously observing at four frequencies, 1.4, 2.3, 4.8, and 8.6 GHz with the ATCA in the 1.5B array. Measured flux densities are given in Table 5. The radio spectrum is inverted with a spectral index of ~ 0.2 . The source shows no polarization above 3 sigma at any of the four frequencies.

One model for ULXs invokes relativistic beaming to account for the high apparent X-ray luminosity (Georganopoulos et al. 2002). The radio flux should also be high in this scenario. However, the X-ray spectra of Galactic and extragalactic jet sources are typically much steeper than that of source # 6 and the observed inverted radio spectrum is not typical of jets which have radio spectral indices near -0.6 (Worrall & Birkinshaw 2004). On the other hand, an inverted spectrum and a lack of polarization are indicative of compact cores of radio galaxies.

4. The Nuclear Region

The nucleus of NGC 5018 is surrounded by an $\sim 15''$ radius (~ 3 kpc) region of unresolved emission. Figure 13 displays the radial profile of the X-ray surface brightness about the nucleus. Also shown is the radial profile of a nearby point source (ULX candidate #3) clearly demonstrating the extended nature of the nuclear emission.

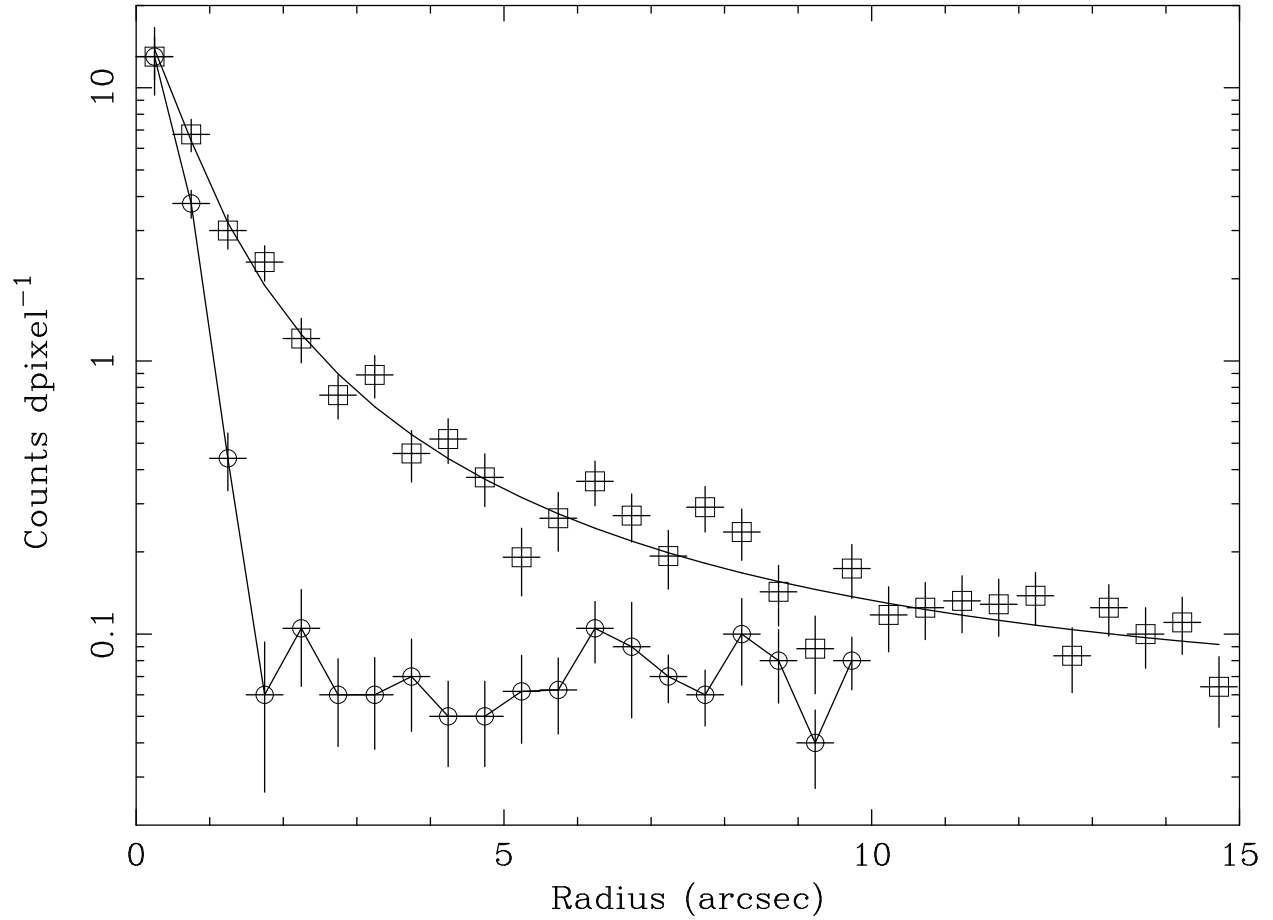


Fig. 13.— Radial profile of the full band (0.5–8.0 keV) X-ray surface brightness about the nucleus of NGC 5018 (open squares). The radial profile of ULX candidate # 3, located 15'' from the nucleus, is also shown for comparison (open circles), which has been scaled to match at the peak. The smooth solid curve represents a standard beta model profile as discussed in the text.

If the nuclear emission is from isothermal gas in hydrostatic equilibrium, then the surface brightness profile would follow a standard beta model, $\propto(1 + (r/r_c)^2)^{-3\beta+1/2}$. Fitting this function (plus a constant representing the background) to the 0.3–8.0 keV X-ray profile out to 15'' from the nucleus results in values of $r_c = 0.''46 \pm 0.''17$ (~ 90 pc), and $\beta = 0.44 \pm 0.02$ ($\chi^2=34.0$ for 27 dof). This function is shown as the smooth curve in Figure 13. The small core radius, r_c , and the low value of β means the profile forms a cusp at the center but is rather flat at larger radii.

The cusp may be due to a true point source at the nucleus; consistent with the identification of a point-like object at that location by our source-finding algorithm. This source has a soft spectrum as shown by its X-ray colors (§ 3.1), but a hard spectral component is often also present in active galactic nuclei. Therefore, the radial profile in the 2–8 keV band was extracted and compared to the full-band profile. The hard-band profile appears more concentrated toward the nucleus (best-fit $r_c = 0.''25 \pm 0.''18$, $\beta = 0.46 \pm 0.04$; $\chi^2 = 32.3$ for 27 dof) compared with the full band profile but is consistent with that profile within errors. It cannot be concluded, based on the surface brightness profiles alone, whether or not there is an X-ray-emitting active nucleus in NGC 5018.

Guided by the known angular size of a point source at the position of the nucleus, we extracted the X-ray spectrum from two regions: One from an annulus extending from 3'' to 20'' around the nucleus and excluding the point sources within this region (henceforth, the extended component), and the other from a disk of radius 3''(the nuclear component). The 20'' outer radius was chosen to roughly correspond to the (spatially-uniform) background level. The spectra were binned to obtain at least 20 counts per fitting bin. A corresponding background spectrum was extracted from a circular annulus that extends from 40'' to 70'' radii, again excluding point sources.

Various XSPEC models were fitted to the extended component spectrum as presented in Table 4 (labeled “Diffuse” in column 1). The spectrum requires at least two spectral components for an acceptable fit. The best fit is a thermal emission line (`mekal`) plus power law model (row 6, Table 4). The abundances of metals is poorly constrained by this model but are consistent with solar values. The spectrum and best-fit model are shown in Figure 14. Extrapolating the luminosity in the 3'' to 20'' annular spectral extraction region to the center of the galaxy using the beta model shape results in a total 0.5–8.0 keV absorption-corrected luminosity of $(1.62 \pm 0.86) \times 10^{40}$ ergs s⁻¹.

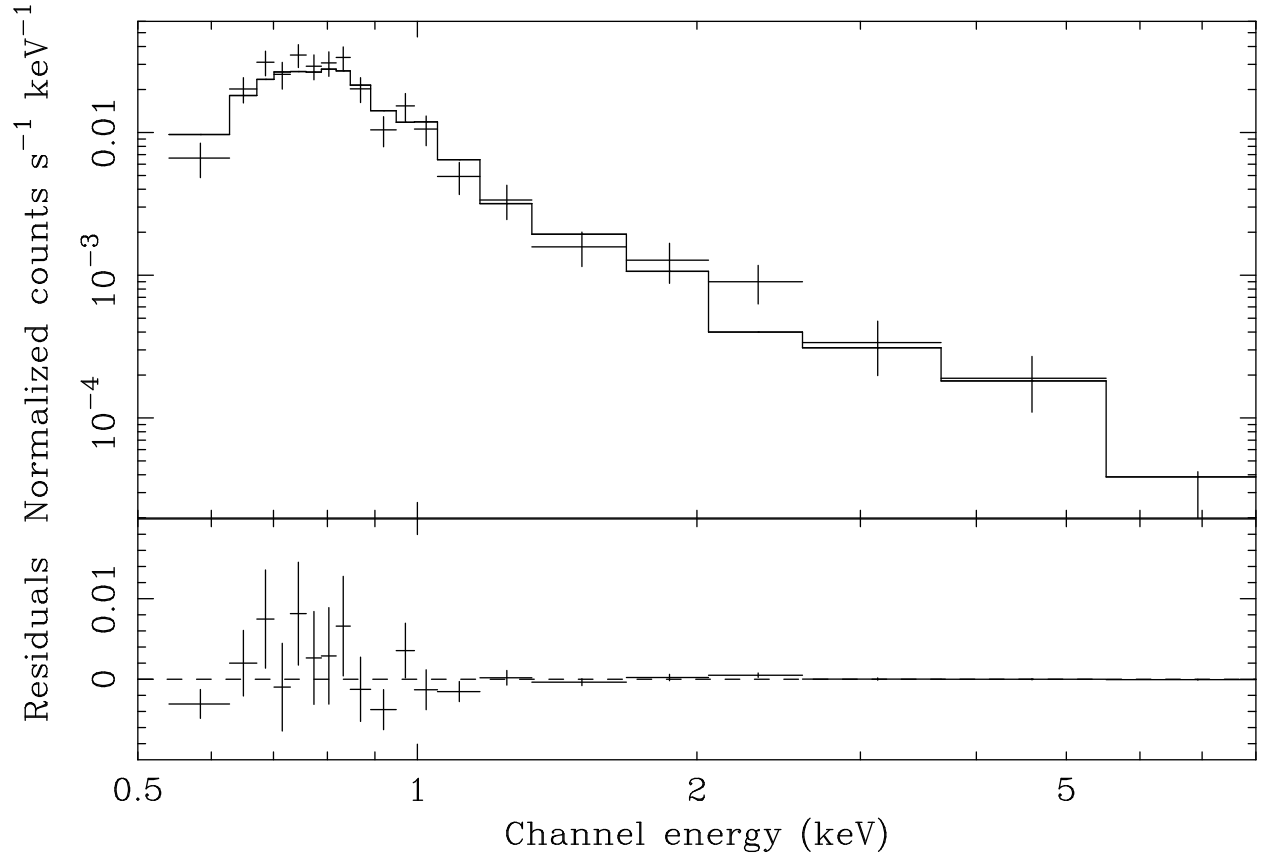


Fig. 14.— X-ray spectrum of the extended, diffuse emission around the nucleus of NGC 5018, extracted from an annulus with 3'' and 20'' radii (upper panel). Also shown are the best-fit model composed of absorbed Mekal and power law components. Fit residuals are shown in the lower panel.

The shape of the extended X-ray spectrum suggests a hot gas origin for the X-ray emission. This is supported by observations at other wavelengths. $H\alpha$ emission has been detected extending to $32''$ (~ 6.3 kpc) from the nucleus with a total luminosity $\sim (6.8 \pm 0.4) \times 10^{39}$ ergs s^{-1} (Goudfrooij et al. 1994). This region also has a distinctly bluer color ($\Delta(B-V) \sim 0.12$ mag) relative to its surroundings (Carollo & Danziger 1994). A portion of the radio emission can also be attributed to an extended source. The total 20 cm continuum emission measured over a $20''$ region around the nucleus is 3.1 ± 0.17 mJy and that from the nucleus itself ($<1''$) is (1.9 ± 0.1) mJy (Mollenhoff et al. 1992). Thus, about 1.2 ± 0.2 mJy is attributable to the extended emission. The radio luminosity is then $\sim (3.6 \pm 0.6) \times 10^{36}$ ergs s^{-1} . This is consistent with our recent radio measurements (Table 5).

Some of the extended X-ray emission may also be due to unresolved point sources. In particular, the hard (power law) spectral component may be produced by LMXBs in the relatively dense core of NGC 5018. The fraction of the extended X-ray emission attributed to this component is 0.46 for a luminosity of $\sim (5.9 \pm 2.9) \times 10^{39}$ ergs s^{-1} . If we assume that of order 10^{37} ergs s^{-1} is an average X-ray luminosity of LMXBs, then ~ 600 unresolved LMXBs are required to account for the hard X-ray emission from the extended component. This is not an unrealistic number of LMXBs in a typical elliptical galaxy. However, a population of LMXBs cannot account for the extended emission observed at other wavelengths. Measured radio luminosities of Galactic LMXBs (e.g., Han & Hjellming 1992; Berendsen et al. 2000; Homan et al. 2004) are only of order $\sim 10^{32}$ ergs s^{-1} and Balmer line emission from LMXB accretion disks is of order a few 10^{32} ergs s^{-1} . Based on these results, we believe that the extended radio, $H\alpha$, and at least 54% of the X-ray emission are from diffuse hot gas in the central regions of NGC 5018.

The spectrum of the nuclear component is also best represented by a two component model (row 8 in Table 4; Figure 15). Of course, we expect a soft component analogous to the soft emission from the surrounding region. Unfortunately, the hard component is also consistent with an extrapolation of the power law emission from beyond the nucleus and so, again, we cannot unequivocally confirm an active nucleus for NGC 5018.

If we assume a nuclear point source is present, then we can compare it to other low luminosity AGNs (LLAGNs). Within $3''$ the power law component contributes 51% of the total luminosity or $L_X = (3.5 \pm 0.7) \times 10^{39}$ ergs s^{-1} . We consider this as the maximum luminosity from any central point source. To obtain a minimum luminosity estimate, we performed a joint fit to the nuclear and extended spectra using a mekal plus powerlaw model. Then, with the constraint that the same parameters are used to fit both spectra, a second power law component was added to the model of the nuclear spectrum only. The 90% confidence upper limit to the contribution from the second powerlaw component is $L_X = 2 \times 10^{37}$ ergs s^{-1} with

a best-fit value of zero. Using these X-ray luminosity limits, the resulting ratio of the 5 GHz flux density (Table 5) to the X-ray luminosity, $\log[\nu L_\nu(5\text{GHz})/L_X]$, is between -2.4 and -0.15. This is within the range of -4.6 to -1.2 typical of LLAGNs (Terashima & Wilson 2003). In addition, the value of $\log(L_X/L_{H\alpha})$ for NGC 5018 is between -1.5 and 0.74 assuming all the $H\alpha$ emission from the $3''$ nuclear region is associated with the point source at the nucleus. Terashima & Wilson (2003) find $\log(L_X/L_{H\alpha})$ for LLAGNs are in the range -0.6 to 2.0.

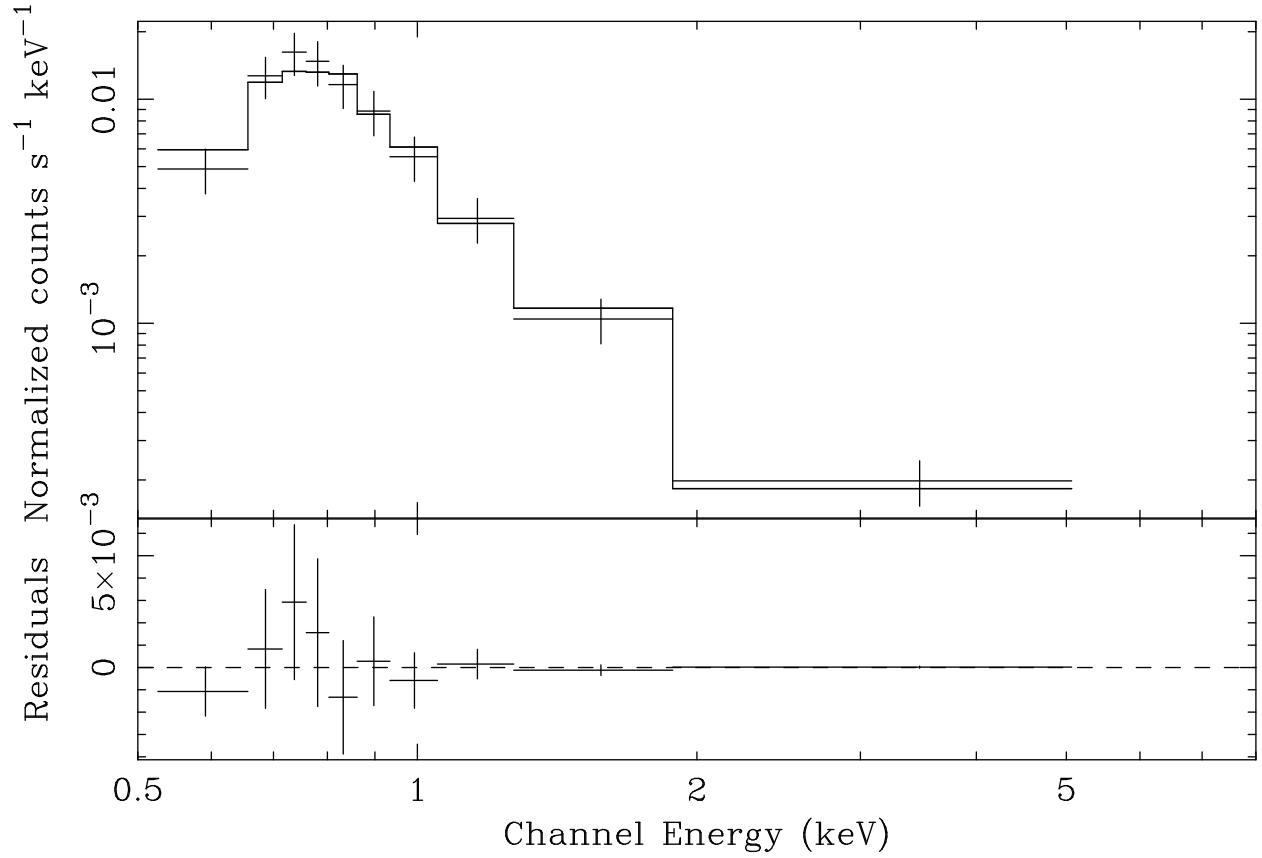


Fig. 15.— X-ray spectrum of the emission within a 3'' radius of the center of NGC 5018. This spectrum is best fitted with an absorbed thermal plus power-law model. Data and the model are shown in the upper panel and the residual between the data and the model is shown in the lower panel of this figure.

There is no evidence for variability of the nuclear emission during the 30 ks *Chandra* observation. The light curve of the hard X-ray emission, >2 keV, is of insufficient quality to determine if the power-law emission component alone is variable.

5. Summary and Discussion

Six non-nuclear X-ray point sources were detected in NGC 5018 in a 30 ks *Chandra* observation. All six sources are potentially ULXs and each displays interesting X-ray and optical properties. An estimated 1.4 sources are background objects.

The dominant contribution to the X-ray point source population in early-type galaxies is LMXBs. Individually, accretion disks and companion stars of LMXBs are too faint at non-X-ray wavelengths to be detectable at the distance of NGC 5018 even with *Hubble*. Sources # 1 and # 4 are in this category. Only upper limits to potential optical counterparts to these sources could be determined and this limit, $M_V \lesssim -6.5$, excludes only the brightest early-type supergiant companions. A better constraint on the companion mass can be made if mass transfer is assumed to be driven by the nuclear evolution of the companion. In this case, the observed X-ray luminosities can be used to constrain the mass transfer rate and hence the companion mass. If the companion is a main sequence star, then it must be more massive than 8 and 20 M_\odot for source # 4 and # 1, respectively (assuming a 10% efficiency converting accreting matter to X-radiation). If the companion is in its giant phase, then these values are reduced to 4 and 8 M_\odot . (Note that these two sources span the range of X-ray luminosities of all the non-nuclear sources so the stellar companions to these other sources also have masses in the range 4 to 20 M_\odot by these arguments.) Stars of such high mass are too short-lived to have been formed at the time of interaction between NGC 5018 and other group member galaxies. Perhaps, as discussed by King (2002), these objects are soft X-ray transients in outburst with emission beamed in the direction of the observer. Alternatively, Bildsten & Deloye (2004) propose ultracompact binaries that can produce very high mass accretion rates from gravitational radiation losses and hence X-ray luminosities in excess of $\sim 5 \times 10^{38}$ ergs s^{-1} .

In any case, the remarkably high X-ray luminosity of source # 1, $>10^{40}$ ergs s^{-1} based on spectral fitting⁴, is perplexing. No model of LMXBs can easily account for such a high X-ray luminosity. Statistically, background objects are most likely to be among the brightest X-ray objects in elliptical galaxy fields (Irwin, Bregman, & Athey 2004). On the other hand,

⁴The X-ray luminosity of source # 1 exceeds that of all 57 ULX candidates detected in 27 elliptical galaxies surveyed by Swartz et al. (2004)

background AGNs tend to have X-ray to optical flux ratios of order unity (e.g., Maccacaro et al. 1988; Green et al. 2004) predicting an optical counterpart to source # 1 far above the *Hubble* detection limit, though none was found for source # 1 (ratio ≥ 186 ; Table 3).

The remaining four sources are all associated with optically bright objects. The (V–I) colors and V magnitudes of these objects are consistent with GCs in NGC 5018 (Hilker & Kissler-Patig 1996). However, source # 3 is likely a background AGN based on its optical variability and source # 6 is likely a background radio galaxy based on its radio signature. Without a spectroscopic redshift confirmation, we cannot be certain if any of these four sources are truly ULXs in NGC 5018 GCs or background objects. Statistically, we expect 1.4 background objects among our 6 ULX candidates, and we expect the X-ray luminosities of the true ULXs to be below $\sim 2 \times 10^{39}$ ergs s $^{-1}$ (Irwin, Athey, & Bregman 2003; Irwin, Bregman, & Athey 2004). Statistically, therefore, sources # 3 and 6 can account for the expected background contribution. In the broader context, we caution that X-ray bright background objects also tend to be optically bright.

In addition to point sources and a possible weak LLAGN, diffuse hot gas has also been detected in the X-radiation from NGC 5018. This gas may be the remnant of interactions of NGC 5018 with its neighbor galaxies. The radiative cooling time of the hot plasma, estimated from the X-ray spectral fit parameters and the size of the emission region, is a few times 10^7 to 10^8 yr, depending on the gas filling factor. This is shorter than the estimated 300 to 600 Myr since the last interaction (Guhathakurta et al. 1989). This suggests the gas is still falling in and/or it is being reheated by ionization, stellar winds, and supernovae from current or recent star formation activity. The current star formation rate (SFR) implied by the H α luminosity is only ~ 0.1 M $_{\odot}$ yr $^{-1}$ but some of this gas is obscured by overlying dust (Goudfrooij et al. 1994). The far-infrared luminosity of NGC 5018 is 2×10^{43} ergs s $^{-1}$ (Thronson & Bally 1987) corresponding to a star formation rate of ~ 0.9 M $_{\odot}$ yr $^{-1}$. This, in turn, may be an overestimate as there is a substantial contribution to the FIR luminosity from dust heated by the interstellar radiation field (Guhathakurta et al. 1989) in addition to the warm component normally associated with young star-forming regions. The mass of atomic and molecular gas in NGC 5018 is $M_{gas} \sim 1.4 \times 10^9$ M $_{\odot}$ (Georgakakis, Forbes, & Norris 2000) implying a gas consumption timescale (M_{gas}/SFR) of order a Hubble time. Thus, while there is little current star formation activity, there is a significant reservoir of gas to maintain this low, steady, level of star formation since the last interaction that may explain the diffuse thermal X-ray (and H α and radio) emission from the central regions of NGC 5018.

We may obtain a broad, though speculative, interpretation of the recent history of NGC 5018 from its X-ray to radio properties. The morphology and radial velocity structure of

the HI gas indicate the interaction between NGC 5018 and NGC 5022 was not a direct impact and merger but an encounter that left the more massive NGC 5018 essentially intact. The interaction did strip gas from NGC 5022 that presently traces the path of the interaction in HI (Kim et al. 1988; Guhathakurta et al. 1989), produced the optical shells (Malin & Hadley 1997), and is currently accreting toward the center of NGC 5018 where it is being heated and ionized. Stars are currently forming out of this gas at a low rate but the rate may have been higher in the recent past if the ULX sources are binaries accreting from normal or giant stars. Within the stellar system is the usual population of LMXBs. Most lie below the point source detection limit in the current *Chandra* data but a number of exceptionally luminous (ULX) candidates are present. These appear to trace the relatively young population of stars contained in blue GCs that may have formed since the last interaction.

Our sincere thanks to the Editor and the referee for their comments that helped to improve the quality of the figures. This research has made use of the NASA/IPAC Extragalactic Database (NED) which is operated by the Jet Propulsion Laboratory, California Institute of Technology, under contract with NASA; of data products from the Two Micron All Sky Survey, which is a joint project of the University of Massachusetts and the Infrared Processing and Analysis Center, funded by NASA and the NSF; from the Multimission Archive (MAST) at the STScI operated by AURA under NASA contract NAS5-26555; and from the Chandra Data Archive, part of the Chandra X-Ray Observatory Science Center (CXC) which is operated for NASA by SAO. The Australia Telescope is funded by the Commonwealth of Australia for operation as a National Facility managed by CSIRO. Support for this research was provided in part by NASA under Grant NNG04GC86G issued through the Office of Space Science.

REFERENCES

- Abramowicz, M. A., Czerny, B., Lasota, J. P., & Szuszkiewicz, E. 1988, *ApJ*, 332, 646.
- Begelman, M. C. 2002, *ApJ*, 568, L97.
- Berendsen, S. G. H. 2000, *MNRAS*, 318, 599.
- Bildsten, L., & Deloye, C. J. 2004, *ApJL*, 607, 119.
- Brandt, W. N. et al. 2001, *AJ*, 122, 2810.
- Carollo, C. M. & Danziger, I. J. 1994, *MNRAS*, 270, 743.

- Colbert, E. J. M., & Mushotzky, R. F. 1999, *ApJ*, 519, 89
- Colbert, E. J. M., & Ptak, A. F. 2002, *ApJS*, 143, 25
- Colbert, E. J. M. et al. 2004, *ApJ*, 602, 231.
- Fabbiano, G., & White, N. 2003, astro-ph/0307077, to appear in “Compact Stellar X-ray Sources,” Cambridge University Press (eds., W. Lewin & M. van der Klis)
- Fabbiano, G. 2004, *RMxAC*, 20, 46.
- Franco, J. et al. 1993, *RevMAA*, 27, 133
- Georgakakis, A., Forbes, D. A. & Norris, R. P. 2000, *MNRAS*, 318, 124.
- Georganopoulos, M., Aharonian, F. A., & Kirk, J. G., 2002 *A&A*, 388, L25
- Gilfanov, M. 2004, astro-ph/0403552, to appear in ”Progress of Theoretical Physics”, Proceedings of the workshop ”Stellar-Mass, Intermediate-Mass, and Supermassive Black Holes”, (Eds: K.Makishima and S.Mineshige.).
- Goudfrooij, P., Hansen, L., Jorgensen, H. E., Norgaard,-Nielsen, H. U., de Jong, T., & van den Hoek, L. B. 1994, *A&AS*, 104, 179
- Green, P. J. et al. 2004, *ApJS*, 150, 43.
- Grimm, H. -J., Gilfanov, M., & Sunyaev, R. 2003, *MNRAS*, 339, 793.
- Guhathakurtha, P., et al. 1989, in “The Interstellar Medium in External Galaxies”, ed. D. J. Hollenbach & A. T. Harley, NASA Conf. Publication 3084, p. 26
- Han, X. & Hjellming, R. M. 1992, *ApJ*, 400, 304.
- Harris, W.E. 1996, *AJ*, 112, 1487
- Hilker, M. & Kissler-Patig, M. 1996, *A&A*, 314, 357.
- Homan, J. 2004, *A&A*, 418, 255.
- Humphrey, P. J. et al. 2003, *MNRAS*, 344, 134.
- Hunter, D. A. et al. 2000, *AJ*, 120, 2383.
- Irwin, J. A., Athey, A. E. & Bregman, J. N. 2003, *ApJ*, 587, 356.
- Irwin, J. A., Bregman, J. N. & Athey, A. E. 2004, *ApJL*, 601, L143

- Kilgard, R. E. et al. 2002, ApJ, 573, 138.
- Kim, D. -W., et al. 1988, ApJ, 330, 684.
- King, A. R., Davies, M. B., ward, M. J., Fabbiano, G., & Elvis, M. 2001, ApJ, 552, L109
- King, A. R. 2002, MNRAS, 335, 13.
- Lotz, J. M. 2004, ApJ, 613, 262.
- Maccacaro, T. et al. 1988, ApJ, 326, 680.
- Makishima, K., et al. 2000, ApJ, 535, 632
- Malin, D. F. & Carter, D. 1983, ApJ, 274, 534
- Malin, D. F. & Hadley, B. 1997, PASA, 14, 82
- Miller, B. W. et al. 1997, AJ, 114, 2381.
- Mollenhoff, C. et al. 1992, A&A, 255, 35.
- Mukai, K. 1993, Legacy, 3, 21.
- Plewa, T. 1995, MNRAS, 275, 143
- Prestwich, A. H., Irwin, J. A. & Boroson, B. 2003, ApJ, 595, 719.
- Roberts, T. P., & Warwick, R. S. 2000, MNRAS, 315, 98.
- Swartz, D. A., Ghosh, K. K., McCollough, M. L., Pannuti, T. G., Tennant, A. F., & Wu, K. 2003, ApJS, 144, 213
- Swartz, D. A., Ghosh, K. K., Tennant, A. F., & Wu, K. 2004, ApJS, 154, 519.
- Tennant, A. F. et al. 2005, in preparation
- Terashima, Y. & Wilson, A. S. 2003, ApJ, 583, 145
- Thronson, H. A. & Bally, J. 1987, ApJL, 319, L63.
- van der Marel, R. P. 2003, astro-ph/0302101
- Veron-Cetty M.P. & Veron P.2003 A&A, 412, 399.
- Whitmore, B. C. et al. 1999, AJ, 118, 1551.

Worrall, D. M. & Birkinshaw, M. 2004, astro-ph/0410297.

Zaggia, S. et al. 1999, A&AS, 137, 75.

TABLE 1
NGC 5018 X-Ray Source Properties

	R.A.		Dec.		Spectral Parameters ^a			L_X^b	$(M - S)/T^c$	$(H - M)/T^c$	Detected Counts, T
	(J2000)		(J2000)		N_H	Γ/kT_e	χ^2/dof	(10^{39} erg s $^{-1}$)			
1	13 12 55.603	-19 30 39.60	$8.7_{-8.7}^{+12.2}$	$1.74_{-0.37}^{+0.43}$	2.1/8	12.9 ± 1.7	$+0.15 \pm 0.06$	-0.19 ± 0.06	233		
2	13 13 01.200	-19 30 57.14	—	—	—	01.0 ± 0.4	$+0.27 \pm 0.17$	-0.13 ± 0.04	18		
3	13 13 02.036	-19 31 05.44	$20.4_{-20.4}^{+25.5}$	$1.26_{-0.4}^{+1.1}$	3.5/2	06.3 ± 0.9	$+0.26 \pm 0.07$	$+0.07 \pm 0.08$	121		
4	13 13 02.708	-19 32 11.56	—	—	—	01.1 ± 0.4	$+0.00 \pm 0.00$	-0.25 ± 0.16	19		
5	13 13 04.343	-19 31 52.62	—	—	—	02.4 ± 0.3	$+0.21 \pm 0.19$	-0.21 ± 0.19	42		
6	13 13 06.476	-19 31 14.82	—	—	—	01.8 ± 0.4	-0.16 ± 0.06	$+0.65 \pm 0.18$	31		
7 ^d	13 13 01.048	-19 31 05.60	6.98	$1.56_{-0.59}^{+0.46}$	3.8/7 ^d	6.8 ± 0.9	-0.70 ± 0.15	$+0.05 \pm 0.04$	115		

^aAbsorption column density unit is 10^{20} cm $^{-2}$; power-law photon index, Γ , given for source 1; disk blackbody temperature, kT_e , for source 3.

^bIntrinsic 0.5–8.0 keV luminosity.

^cColors from S (0.5–1.0 keV), M (1.0–2.0 keV) and H (2.0–8.0 keV) bands.

^dNucleus. Total counts from the 3'' region is 226. Mekal temperature is 0.33 ± 0.1 keV.

TABLE 2
Hubble observations of NGC 5018

Date of observations	Dataset #	File name	Filter	Exposure (s)	Offset		ULXs ^a
					$\Delta\alpha(^{\circ})$	$\Delta\delta(^{\circ})$	
7-29-1995	1	U2ST0201B	F336W	1800	0.018	0.6	1,2,3
7-28-1997	2	U3M72505B	F555W	1200	0.002	0.4	1,2,3
2-04-1999	3	U5710401B	F555W	4440	0.028	0.5	2,3,4,5,6
7-28-1997	4	U3M72508B	F814W	1900	0.022	0.5	1,2,3
2-04-1999	5	U5710407B	F814W	5240	0.042	0.1	2,3,4,5,6

^aPositions of ULXs covered in the image.

TABLE 3
The measured photometric magnitudes of counterparts of 6 ULX candidates in NGC 5018

ULX (#)	HST data- set #	Chandra error circle radius (")	F336W ^a mag	F555W ^a (mag)	F814W ^a (mag)	M_V^b (mag)	$(V - I)^b$ (mag)	F_X/F_O
1	3,5	0.15	—	27.1±1.2	26.9±1.9	-6.5±1.2	-0.1±2.2	186.0
2	2,4	0.10	—	25.5±0.7	24.0±0.4	-8.0±0.7	1.3±0.8	2.8
2	3,5	0.10	—	25.3±0.5	23.7±0.3	-8.2±0.5	1.4±0.6	2.3
3	1	0.10	22.4±0.1	—	—	—	—	—
3	2,4	0.10	—	23.3±0.2	22.1±0.1	-10.2±0.2	1.0±0.2	2.2
3	3,5	0.10	—	22.2±0.1	21.2±0.1	-11.3±0.1	0.9±0.1	0.8
4	3,5	0.16	—	27.4±1.2	26.9±1.5	-6.1±1.2	0.3±1.9	17.4
5	3,5	0.20	—	23.5±0.2	22.7±0.2	-9.9 ±0.2	0.7±0.3	1.1
6	3,5	0.20	—	24.0±0.2	22.8±0.1	-9.5±0.2	1.0±0.3	1.1

^aObserved magnitudes, not Galactic extinction corrected.

^b M_V means Galactic extinction-corrected ($N_H=6.98 \times 10^{20} \text{ cm}^{-2}$, $N_H/E(B-V)=5.2 \times 10^{21} \text{ cm}^{-2} \text{ mag}^{-1}$ and $A/E(B-V)=3.315$ for V and 1.940 for I) absolute magnitude at F555W band. Similarly, $(V-I)$, is the difference in extinction-corrected magnitudes in F555W, and F814W.

TABLE 4
X-Ray Spectral Parameters of the nucleus and the diffuse emission in NGC 5018

Source	Model	N_H (10^{20} cm^{-2})	Γ	kT_e (keV)	L_X^a ($10^{39} \text{ erg s}^{-1}$)	χ^2/dof
Diffuse	pha * Power-law	65.9 ^{+17.6} _{-30.8}	6.8 ^{+1.0} _{-1.5}	—	124.3±17.8 ^b	129.3/30
Diffuse	pha * Bremsstrahlung	45.7 ^{+22.6} _{-26.4}	—	0.20 ^{+0.01} _{-0.01}	43.7±27.8 ^b	103.9/30
Diffuse	pha * Mekal	7.1 ^{+6.2} _{-6.5}	—	0.44 ^{+0.05} _{-0.07}	7.6±1.7 ^b	51.2/30
Diffuse	pha * (Mekal + Mekal)	6.98 ^{+0.0} _{-0.0}	0.43 ^{+0.11} _{-0.13} ^c	0.43 ^{+0.05} _{-0.05}	7.9±2.8 ^b	51.3/29
Diffuse	pha * (Mekal + Power-law)	6.98	1.06 ^{+0.43} _{-0.45}	0.41 ^{+0.04} _{-0.04}	13.7±1.5 ^b	27.1/29
Nucleus	pha * Mekal	41.2 ^{+17.5} _{-23.5}	—	0.26 ^{+0.07} _{-0.06}	20.7±3.9 ^a	33.5/8
Nucleus	pha * Power-law	59.6 ^{+20.8} _{-24.9}	6.3 ^{+1.3} _{-2.8}	—	50.6±6.9 ^a	43.4/8
Nucleus	pha * (Mekal + Power-law)	6.98	1.56 ^{+0.46} _{-0.59}	0.39 ^{+0.08} _{-0.09}	6.8±0.9 ^a	3.8/7

^aIntrinsic 0.5–8.0 keV luminosity in the 0-3'' region.

^bIntrinsic 0.5–8.0 keV luminosity in the 3''-20'' region.

^cTemperature of the second Mekal component in keV.

TABLE 5
Radio continuum measurements of NGC 5018

Source	R.A. (1950)	Dec. (1950)	S_P^a (mJy)	S_T^a (mJy)	3 cm (mJy)	6 cm (mJy)	13 cm (mJy)	22 cm (mJy)	Angular size (")	Refer- ence
Nucleus	13 10 19.9(1)	-19 15 14(10)	—	3.3 ± 0.50	—	—	—	—	L	1
Nucleus	13 10 20.00	-19 15 11.0	—	3.1 ± 0.17	—	—	—	—	< 20	2
Nucleus	13 10 20.04	-19 15 12.5	1.9 ± 0.1	1.9 ± 0.10	—	—	—	—	< 1	2
Nucleus	13 10 20.05	-19 15 11.9	—	—	0.9 ± 0.1	1.4 ± 0.1	1.9 ± 0.1	2.0 ± 0.1	< 3	3
ULX # 6	13 10 25.3(0.7)	-19 15 26(10)	—	3.3 ± 0.50	—	—	—	—	L	1
ULX # 6	13 10 25.50	-19 15 26.0	—	2.5 ± 0.17	—	—	—	—	< 20	2
ULX # 6	13 10 25.45	-19 15 21.5	4.0 ± 0.2	4.0 ± 0.20	—	—	—	—	< 1	2
ULX # 6	13 10 25.47	-19 15 21.2	—	—	3.0 ± 0.1	3.1 ± 0.1	2.3 ± 0.2	2.1 ± 0.3	< 3	3

^a20 cm, L: low resolution, 1:Kim et al. 1988, 2:Mollenhoff et al. 1992 and 3: this work